



1 **Recent glacier mass balance and area changes in the Kangri Karpo**
2 **Mountain derived from multi-sources of DEMs and glacier**
3 **inventories**

4
5 Wu Kunpeng^{1,2}, Liu Shiyin^{2,3*}, Jiang Zongli⁴, Xu Junli⁵, Wei Junfeng⁴, Guo Wanqin²

6 ¹School of Resources and Environment, Anqing Normal University, Anqing, Anhui, China

7 ²State key Laboratory of Cryospheric Sciences, Northwest Institute of Eco-Environment and Resources, Chinese Academy of Sciences,
8 Lanzhou, China

9 ³Institute of International Rivers and Eco-Security, Yunnan University, Yunnan, China

10 ⁴Department of Geography, Hunan University of Science and Technology, Xiangtan, China

11 ⁵Department of Surveying and Mapping, Yancheng Teachers University, Yancheng, China

12 Correspondence to LIU Shiyin at liusy@lzb.ac.cn or WU Kunpeng at wukunpeng2008@lzb.ac.cn

13
14 **Abstract.** Due to the effect of Indian monsoon, the Kangri Karpo Mountain, located in southeast
15 Tibetan Plateau, is the most humid region of Tibetan Plateau, and become one of the most
16 important and concentrated regions with maritime (temperate) glaciers development. Glacier mass
17 loss in Kangri Karpo Mountain is important contributor to global mean sea level rise, and it
18 change runoff distribution, increase risk of glacial lake outburst floods (GLOFs). Because of their
19 difficult accessibility and high labor costs, the knowledge of glaciological parameters of glaciers
20 in the Kangri Karpo Mountain is still limited. This study presents glacier elevation changes in the
21 Kangri Karpo Mountain, by utilizing geodetic methods based on digital elevation models (DEM)
22 derived from Topographic Maps (1980), the Shuttle Radar Topography Mission (SRTM) DEM
23 (2000), and TerraSAR-X/TanDEM-X (2014). Glacier area and length changes were derived from
24 Topographical Maps and Landsat TM/ETM+/OLI images between 1980 and 2015. Our results
25 show that the Kangri Karpo Mountain contains 1166 glaciers, with an area of $2048.50 \pm 48.65 \text{ km}^2$
26 in 2015. Ice cover in the Kangri Karpo Mountain diminished by $679.51 \pm 59.49 \text{ km}^2$ ($24.9\% \pm$
27 2.2%) or $0.71\% \pm 0.06\% \text{ a}^{-1}$ from 1980–2015, however, with nine glaciers in advance from 1980–
28 2015. Glaciers with area of 788.28 km^2 in the region, as derived from DEM differencing, have
29 experienced a mean mass deficit of $0.46 \pm 0.08 \text{ m w.e. a}^{-1}$ from 1980–2014. These glaciers showed
30 slight accelerated shrinkage and significant accelerated mass loss during 2000–2015 compared to
31 that during 1980–2000, which is consistent with the tendency of climate warming.

32
33 **1 Introduction**

34 Glaciers in the Tibetan Plateau (TP), as a key components in cryosphere system (Li et al., 2008),
35 are the water resource of many major rivers and lakes (Immerzeel et al., 2010). Glacier mass
36 balance is a valuable indicator to understand the climate variability on the TP (Oerlemans, 1994;
37 Yao et al., 2012a). Under the background of global warming, many mountain glaciers have
38 progressively shrunk in mass and extent in past decades (IPCC, 2013). However, glaciers with
39 positive mass balance have also been reported in recent years, especially in the central Karakoram,
40 eastern Pamir and the western TP (Bao et al., 2015; Gardelle et al., 2012b; Gardelle et al., 2013;
41 Kääb et al., 2015; Neckel et al., 2014; Yao et al., 2012a). The relationship between glacier mass



1 balance and climate change, and the knowledge of water source in cryosphere and its disaster risks,
2 are become an advanced research hotspot.

3 Glaciers in the Kangri Karpo Mountain is known as temperate characteristic under a warming
4 climate and abundant precipitation from Indian Monsoon (Li et al., 1986; Shi and Liu, 2000).
5 Literature review shows the lack of studies of glacier changes in the Kangri Karpo Mountain on a
6 longer time scale, especially the studies of mass balance. Based on digitized glacier inventories
7 from Topographic Maps and remote sensing images, or in situ measurements, glaciers in the
8 Kangri Karpo Mountains have experienced an intense area reduction, mass deficit, and continued
9 terminus retreat (Li et al., 2014; Yang et al., 2010; Yang et al., 2008; Yao et al., 2012a). While
10 some previous studies showed that the phenomenon of glacier advance exists in the Kangri Karpo
11 Mountain. Based on aerial photographs, China – Brazil Earth Resources Satellite (CBERS) image
12 and Landsat Thematic Mapper (TM) image, about 60% of glaciers in the region have been losing
13 their mass and other glaciers have advanced during 1980 to 2001 (Liu et al., 2006). Shi et al.
14 (2006) attributed the complex behavior of glacier dynamics to the increase of precipitation
15 suppressing glacier melting.

16 Although glacier mass deficit was established, the results did differ from each other (Gardelle
17 et al., 2013; Gardner et al., 2013; Kääb et al., 2015; Neckel et al., 2014). Using SRTM DEM and
18 SPOT5 DEM (24 November 2011), glaciers experienced a mean thinning of $0.39 \pm 0.16 \text{ m a}^{-1}$ in
19 eastern Nyainqentanglha Mountains (Gardelle et al., 2013). Based on ICESat and SRTM, (Kääb et
20 al., 2015), (Neckel et al., 2014) and (Gardner et al., 2013) acquired different results over eastern
21 Nyainqentanglha Mountain, with glacier thickness loss of $1.34 \pm 0.29 \text{ m a}^{-1}$, $0.81 \pm 0.32 \text{ m a}^{-1}$ and
22 $0.30 \pm 0.13 \text{ m a}^{-1}$, respectively.

23 Glacier mass balance can be acquired through glaciological, hydrological and geodetic
24 methods (Ye et al., 2015). Due to high altitude and harsh climatic conditions, it is hard to carry out
25 widespread in-situ measurements. Meanwhile, satellite remote sensing is a promising alternative
26 to conduct glacier mass balance through geodetic method, even in remote mountainous terrains
27 and over several glaciers at a time (Paul and Haeberli, 2008). Glaciers in the Kangri Karpo
28 Mountain were almost completely mapped by Topographic Maps that made from aerial
29 photographs in October 1980, and then mapped by X-band SAR Interferometry (InSAR) in
30 February 2000 during the SRTM resulting in a Digital Elevation Model. Glaciers in the region were
31 mapped again by single-pass X-band InSAR from TerraSAR-X on 18 February 2014 and 13 March
32 2014, and its add-on for digital elevation measurements (TanDEM-X) (Krieger et al., 2007). In
33 this study, the approach of Differential Synthetic Aperture Radar Interferometry (DInSAR) was
34 used to estimate glacier mass balance in the Kangri Karpo Mountain between 1980 and 2014.

35 2 Study Area

36 The Kangri Karpo Mountain, located on the eastern end of the Nyainqentanglha Mountains in
37 southeast Tibetan Plateau, extent about 280 km from northwest to southeast. This region located in
38 the south of Bomi County, and near to Motuo, Zayu and Basu County (Fig. 1). The north of this
39 region, Purlung Zangbo, is a tributary of the Yalung Zangbo River, and the other side is Gongri
40 Gabo River which belongs to west tributary of the Zayu River. Because the east section faces the
41 entrance of the moist southwest monsoon from Indian Ocean, which enters into the plateau at the
42 Grand Bend of the Yarlung Zangbo River, and the terrain forces the air flow to rise, it is the region
43 with the maximum precipitation and highest moisture on the plateau and hence glaciers are
44 well-developed (Shi et al., 2008a).



1 During winter and spring, the westerly jet in the Northern Hemisphere was blocked by
2 Tibetan Plateau and divided into two branches, southern branch develops into a trough in study
3 area after bypassing the Himalaya Mountains. Moisture in the Bay of Bengal region was attracted
4 by the trough, land on TP and form strong snowfall. In summer, due to the effect of topography
5 flattening, abundant precipitation was transported to study area by the Indian monsoon (Li et al.,
6 1986). Hence, the Kangri Karpo Mountain is the most humid region of Tibetan Plateau, and
7 become one of the most important and concentrated regions with maritime (temperate) glaciers
8 development (Shi and Liu, 2000). It is estimated that the mean summer air temperature at the
9 equilibrium-line altitude (ELA) of glaciers in the region is usually above 1 °C, and annual
10 precipitation is about 2500–3000 mm (Shi et al., 1988). Most glaciers in study area are in the state
11 of pressure melting point, glacier surface ablation is intensive and the velocity of glacier
12 movement is fast (Li et al., 1986).

13 According to the first Chinese Glacier Inventory, the Kangri Karpo Mountain contains 1320
14 glaciers, with a total area and volume of 2655.2 km² and 260.3 km³, respectively (Mi et al., 2002).
15 Yalong Glacier (CGI code: 5O282B37) is the largest one among these glaciers (191.4 km² in
16 surface area and 32.5 km long), while the Ata Glacier (CGI code: 5O291B181), located on the
17 south slope of the Kangri Karpo Mountain, is the glacier with the lowest terminus at 2450 m, 16.7
18 km in length and 13.75 km² in area (Liu et al., 2006). Comparison of photographs taken in
19 different time found that tongue position of Ata Glacier, ice volume and glacial surface conditions
20 have changed greatly in the past decades (Yang et al., 2008).

21

22 3 Data

23 3.1 Topographic Maps

24 Five topographic maps on 1:100000 scale and fifty topographic maps on 1:50000 scale generated
25 from aerial photos acquired in October 1980 by the Chinese Military Geodetic Service was
26 employed in the present study. Using a seven parameter transformation method, these maps
27 georeferenced into the 1954 Beijing Geodetic Coordinate System (BJ54) with geoid (datum level
28 is Yellow Sea mean sea level at Qingdao Tidal Observatory in 1956) were re-projected into World
29 Geodetic System 1984 (WGS1984)/Earth Gravity Model 1996 (EGM96) (Xu et al., 2013). The
30 contour lines of the maps were manually digitized and then converted into raster DEM (TOPO
31 DEM) with a 30 m grid cell by employing the Thiessen polygon method (Shangguan et al., 2010;
32 Wei et al., 2015b; Zhang et al., 2016a). According to the national photogrammetrical standard of
33 China (GB/T12343.1, 2008), the vertical accuracy of the TOPO DEM is better than 9 m on
34 glaciers with gentle slopes (~19 °) which is common for most of the glacierized areas in the Kangri
35 Karpo Mountain.

36 3.2 Shuttle Radar Topography Mission

37 The SRTM was conducted to acquire interferometric synthetic aperture radar (InSAR) data
38 simultaneously in the C-band and X-band frequencies from 11 to 22 February 2000 (Farr et al.,
39 2007). The SRTM DEM can be referred to the glacier surface in the last balance year (1999) with
40 slight seasonal variances (Gardelle et al., 2013; Pieczonka et al., 2013; Zwally et al., 2011). The
41 X-band SAR system was operated with a swath width of 45 km leaving large data gaps in the
42 resulting X-band DEM (Rabus et al., 2003). Unfortunately, only 23% of the Kangri Karpo glaciers
43 are covered by the data set. The unfilled finished SRTM C-band DEM, with a swath width of 225



1 km and 1 arc-second resolution (approximately 30 m) in WGS84/EGM96, is freely available for scientific purposes (<http://earthexplorer.usgs.gov/>). Hence, the unfilled finished SRTM C-band DEM was employed to study ice surface elevation change.

4 3.3 TerraSAR-X/TanDEM-X

5 TerraSAR-X was launched in June 2007 by the German Aerospace Center (DLR). TerraSAR-X and its add-on for digital elevation measurements (TanDEM-X) are flying in a close orbit formation acting as a flexible single-pass SAR interferometer (Krieger et al., 2007). Interferometric data acquisition can be performed in the pursuit monostatic mode, the bistatic mode and the alternating bistatic mode. Current baseline for operational DEM generation is the bistatic mode which minimizes temporal decorrelation and makes efficient use of the transmit power (Krieger et al., 2007).

12 The experimental Co-registered Single look Slant range Complex (CoSSC) files, acquired in bistatic InSAR stripmap mode on 18 February 2014 and 13 March 2014, were employed in this study (Fig. 2 and Table 1). The CoSSC files have been focused and co-registered at the TanDEM-X Processing and Archiving Facility (PAF). The GAMMA SAR and interferometric processing software was employed for the interferometric processing of the CoSSC files (Werner et al., 2000).

17 3.4 Landsat images

18 In order to analyze the relationship between glacier mass balance and changes in glacier extent, two Landsat Thematic Mapper (TM) scenes, one Landsat Enhanced Thematic Mapper Plus (ETM+) scene and three Landsat Operational Land Imager (OLI) scenes were employed in this study (Table 1). It is better that Landsat images were acquired in the same year with SRTM and TerraSAR-X/TanDEM-X acquisitions, while because of the low quality of Landsat images in 2000 and 2014, Landsat TM/ETM+ images in 2001 and Landsat OLI images in 2015 with high quality were selected in this study. All Landsat images are available from the United States Geological Survey (USGS), and are orthorectified with the SRTM and ground control points from the Global Land Survey 2005 (GLS2005) dataset. Amongst the Landsat images, the co-registered TerraSAR-X coherence image, the SRTM-X DEM and Topographic Maps, almost no horizontal shift was observed. For Landsat ETM+/OLI images, pan-sharpening employing principal component analysis was performed to enhance the spatial resolution to 15 m.

31 4 Methods

32 4.1 Glacier Inventory

33 The outlines of glaciers in October 1980 were delineated manually from Topographic Maps. These maps were geo-referenced and rectified with a kilometer grid, and validated by reference to the original aerial photographs to update the first Chinese Glacier Inventory (Wu et al., 2016b).

36 Global inventory of glacier outlines can be available through the Randolph Glacier Inventory (Arendt et al., 2015). For the Kangri Karpo Mountain, these glacier outlines are taken from “the Second Chinese Glacier Inventory” (CGI2) that delineated from Landsat TM on 8 September 2005 (Guo et al., 2015). An inventory of high-mountain Asian glaciers named “Glacier Area Mapping for Discharge from the Asian Mountains” was compiled from 356 Landsat ETM+ scenes in 226 path-row sets (Nuimura et al., 2015). The GAMDAM outlines are nearly all from 1999-2003 and thus conform with the recommendation for the compilation of glacier inventory to



1 select imagery as close to 2000 as possible (Arendt et al., 2015; Paul et al., 2009). Hence, Landsat
2 TM/ETM+ scenes were used to validate and update the CGI2 and GAMDAM glacier inventory,
3 and generated the 2000 inventory of the detailed study area.

4 A semi-automated approach using the TM3/TM5 band ratio was applied to delineate glacier
5 outlines in 2015 using Landsat OLI images (Bolch et al., 2010b; Paul et al., 2009; Racoviteanu et
6 al., 2009). To ensure that ice patches were larger than 0.01 km², a 3 by 3 median filter was applied
7 to eliminate isolated pixel (Bolch et al., 2010b; Wu et al., 2016b). Then, the derived glacier
8 polygons are checked manually against images from adjacent years with less or no snow and
9 cloud-free, to discriminate proglacial lakes, seasonal snow, boulders on the glacier and
10 debris-covered ice (Fig. 3). The final contiguous ice coverage was divided into individual glacier
11 polygons using topographical ridgelines (TRLs), which were automatically generated based on the
12 SRTM-C DEM (Guo et al., 2011).

13 The best way to assess the accuracy of glacier outlines is to compare extracted results with
14 independently digitized glacier outlines from high resolution aerial imagery at random locations
15 (Bolch et al., 2010a; Paul et al., 2003). Previous studies indicated that the average offsets between
16 glacier outlines derived from Topographic Maps and Corona-image outlines was ± 6.8 m (Wu et al.,
17 2016b), and the average offsets between Landsat-image outlines and real-time kinematic
18 differential GPS (RTK-DGPS) measurements, Google EarthTM images with a spatial resolution
19 better than 1 m, were ± 10 m and ± 30 m for the delineation of clean and debris-covered ice,
20 respectively (Guo et al., 2015). On the basis of these average offsets, mean relative errors of
21 $\pm 1.3\%$, $\pm 2.0\%$ and $\pm 2.4\%$ were calculated for glacier area in 1980, 2000 and 2015, respectively.

22 4.2 Glacier Length

23 Glacier length is a key parameter in glacier inventory and its vector representation (glacier
24 centerlines) is important to model future glacier evolution and calculate glacier ice volume (Le
25 Bris and Paul, 2013). Some researchers defined it as the central flowline from the highest glacier
26 elevation to the terminus, whereas others regard the length of the longest flowline as glacier length
27 (Kienholz et al., 2014; Leclercq et al., 2014). The length change can be calculated by intersecting
28 the central flowline with the respective glacier outline (Paul and Svoboda, 2010), or calculated as
29 the average length from the intersection of the glacier outlines with the stripes which drawn
30 parallel to the main flow direction of the glaciers (Koblet et al., 2010).

31 In this study, a new strategy based on a glacier axis concept from glacier morphology
32 perspective was applied that requires only glacier outlines and a DEM as input (Yao et al., 2015).
33 An error estimation of the resulting glacier centerlines was performed that compared the
34 semi-automatically generated results to high resolution aerial imagery at the terminus of glacier
35 centerlines. A Corona image with a resolution of 4 m and Google EarthTM images with a resolution
36 better than 1 m were used to evaluate the accuracy of glacier centerlines. Hence, the uncertainties
37 of glacier centerlines from Topographic Maps and Landsat images are no more than 6 m and 7.5 m,
38 respectively.

39 4.3 Glacier elevation changes

40 The TerraSAR-X/TanDEM-X acquisitions were processed by differential SAR interferometry
41 (DInSAR) (Neckel et al., 2013) using GAMMA SAR and interferometric processing software
42 (Werner et al., 2000). In order to improve the phase-unwrapping procedure and minimize errors,
43 the unfilled finished SRTM C-band DEM were employed in this study. Before generating the



1 differential interferogram, precise horizontal offset registration and fitting between the SRTM
2 C-band DEM and the TerraSAR-X/TanDEM-X acquisitions is necessary. Based on the relation
3 between the map coordinates of the SRTM C-band DEM segment covering the
4 TerraSAR-X/TanDEM-X master file, and the SAR geometry of the respective master file, an
5 initial lookup table was calculated. While the areas of radar shadows and layover in the
6 TerraSAR-X/TanDEM-X interferogram would induce gaps in the lookup table, a method of linear
7 interpolation between the gap edges in each line of the lookup table was used to fill these gaps.
8 The offsets between the master scene and the simulated intensity of the SRTM C-band DEM, were
9 calculated using cross correlation optimization of the simulated SAR images employing
10 *GAMMA's offset_pwrn* module. The horizontal registration and geocoding lookup table were
11 refined by these offsets. The SRTM C-band DEM was translated from geographic coordinates into
12 SAR coordinates via the refined geocoding lookup table, and conversely, the final difference map
13 was translated from SAR coordinates into geographic coordinates. Then a differential
14 interferogram was generated by the TerraSAR-X/TanDEM-X interferogram and the simulated
15 phase of the co-registered SRTM C-band DEM. An adaptive filtering approach was used to filter
16 the differential interferogram (Goldstein and Werner, 1998), and then *GAMMA's* minimum cost
17 flow (MCF) algorithm was employed to unwrap the flattened differential interferogram.
18 According to the computed phase-to-height sensitivity and select ground control points (GCPs)
19 from the respective off-glacier pixel locations in the SRTM C-band DEM, the unwrapped
20 differential phase was converted to absolute differential heights. While, a residual not covered by
21 the baseline refinement would be existed, and can be regarded as a linear trend that estimated by a
22 two dimensional first order polynomial fit in off-glacier regions. The linear trend and a constant
23 vertical offset were removed from the maps of absolute differential heights. Finally, the resulting
24 data sets were translated to a metric cartographic coordinate system with $30\text{ m} \times 30\text{ m}$ pixel
25 spacing (Neckel et al., 2013). The same method of DInSAR was employed to acquire the glacier
26 elevation change from 1980 to 2014 with the data sets of TOPO DEM and
27 TerraSAR-X/TanDEM-X acquisitions.

28 For the glacier elevation change from 1980 to 1999, a difference map was constructed by
29 common DEM differencing with TOPO DEM and SRTM C-band DEM (Bolch et al., 2011; Nuth
30 and Kääb, 2011; Pieczonka et al., 2013; Wei et al., 2015a). Relative horizontal and vertical
31 distortions between the two data sets, can be corrected by statistical approaches that based on the
32 relationship between elevation difference and slope, aspect (Nuth and Kääb, 2011). Elevation
33 differences in off-glacier regions were used to analyze the consistency of TOPO DEM and SRTM
34 C-band DEM (Fig. 4). Outliers of elevation differences, usually around data gaps and near DEM
35 edges, were omitted with values exceeding $\pm 100\text{ m}$ (Berthier et al., 2010; Bolch et al., 2011). The
36 vertical biases and horizontal displacements could be adjusted simultaneously using the
37 substantial cosinusoidal relationship between standardized vertical bias and topographical
38 parameters (slope and aspect). And the biases that caused by different spatial resolutions between
39 DEMs, could be adjusted by the relationship between elevation differences and maximum
40 curvatures (Gardelle et al., 2012a; Nuth and Kääb, 2011).

41 The penetration depth of SRTM C-band radar beam into snow and ice need to be considered
42 for elevation changes of glacier surfaces (Berthier et al., 2006; Gardelle et al., 2012a; Pieczonka et
43 al., 2013). Penetration depth can range from 0 to 10 m depending on a variety of parameters such
44 as snow temperature, density and water content (Berthier et al., 2006; Dall et al., 2001). As a first



1 approximation, the penetration depth of SRTM X-band radar beam is much smaller than C-band,
2 the elevation difference between these two data sets can be considered as the penetration of SRTM
3 C-band radar beam into snow and ice (Gardelle et al., 2012a). The elevation differences between
4 SRTM C-band and X-band indicate that the penetration depth of the C-band averaged 1.24 m
5 in the study area. The mean value of the SRTM C-band penetration over glaciers in Kangri
6 Karpo Mountain is in agreement with (Gardelle et al., 2013), who found penetration of 1.7 m
7 in eastern Nyainqentanglha Mountains (named Hengduan Shan in (Gardelle et al., 2013)).

8 **4.4 Mass balance and error estimation**

9 In order to convert the derived surface elevation changes into the mass balance of glaciers, a
10 density of ice/firn/snow should be considered. A value of 900 kg m^{-3} was applied to assess the
11 mass changes in water equivalent (w.e.) from elevation differences, and then adding an ice density
12 uncertainty of 17 kg m^{-3} .

13 For the accuracy assessment of TOPO DEM and SRTM C-band DEM, the elevation product
14 of Geoscience Laser Altimeter System (GLAS) carried on-board the Ice Cloud and Elevation
15 Satellite (ICESat) was utilized in this study (Neckel et al., 2013). All available GLAS elevation
16 data for the study area were obtained from the National Snow and Ice Data Center (NSIDC)
17 (release 634; product GLA 14). Because of the effect of clouds during the time of data acquisition,
18 some GLAS elevation data cannot represent the true altitude of ground surface. Outliers of
19 elevation difference between GLA 14 and multi-source of DEMs in off-glacier regions were
20 removed from the analysis with values exceeding $\pm 100 \text{ m}$. Compared to the GLAS elevation data,
21 a mean and standard deviation of $2.74 \pm 1.73 \text{ m}$ and $2.65 \pm 1.48 \text{ m}$ for TOPO DEM and SRTM
22 C-band DEM, respectively. Due to the GCPs that convert the unwrapped
23 TerraSAR-X/TanDEM-X interferogram into absolute heights was selected from the respective
24 off-glacier pixel locations in the SRTM C-band DEM, vertical bias of TerraSAR-X/TanDEM-X
25 DEM and GLA 14 is similar with the bias of SRTM C-band DEM and GLA 14.

26 For an error estimate of the derived surface elevation changes, the residual elevation
27 differences were estimated in off-glacier regions assuming that these areas did not change in
28 height between 1980 and 2014 and that elevations should be equal in TOPO DEM, SRTM C-band
29 DEM and TerraSAR-X/TanDEM-X DEM. The mean elevation difference (MED) over off-glacier
30 regions between the final difference maps was in the range of -1.42 to 0.75 m (Table 2). Because
31 averaging over larger regions reduces the errors, the standard deviation (STDV) over off-glacier
32 regions would probably overestimate the uncertainty for larger samples. Thus, the uncertainty can
33 be estimated by the standard error of the mean (SE):

$$34 \quad SE = \frac{STDV}{\sqrt{N}} \quad (1)$$

35 where N is the number of the included pixels. To avoid the effect of autocorrelation,
36 de-correlation length of 600 m and 200 m was employed for difference maps that derived by
37 common DEM differencing and DInSAR (Bolch et al., 2011; Neckel et al., 2013). Then, the
38 overall errors of the derived surface elevation changes can be estimated using SE and MED
39 over off-glacier regions:

$$40 \quad \sigma = \sqrt{MED^2 + SE^2} \quad (2)$$

41 Finally, the root of sum of squares of the estimated errors of glacier area and surface
42 elevation changes, and ice density uncertainty of 17 kg m^{-3} , were used to estimate the overall
43 errors of mass balance (Neckel et al., 2013).



1 5 Results

2 5.1 Area change

3 According to the 2015 inventory, the Kangri Karpo Mountain contains 1166 glaciers, with an area
4 of $2048.50 \pm 48.65 \text{ km}^2$, and the mean glacier size is about $1.76 \pm 0.04 \text{ km}^2$ (Fig. 5). The highest
5 number of glaciers can be found in the size class $0.1\text{-}0.5 \text{ km}^2$, whereas glaciers between $1\text{-}5 \text{ km}^2$
6 cover the largest area (Fig. 5A). Only two glaciers area larger than 50 km^2 , the largest glacier is
7 Yalong Glacier and another is Xirinongpu Glacier, with glacier area of $173.00 \pm 0.67 \text{ km}^2$ and
8 $90.28 \pm 0.23 \text{ km}^2$, respectively. Glaciers area in Kangri Karpo Mountain present a normal
9 distribution in different elevation, about 76.9% of glacier area lies in the 4500-5500 m elevation
10 range. Azha Glacier is the glacier with the lowest glacier tongue position, and the elevation of
11 glacier tongue at 2551 m (Fig. 5B). Median elevation of the glaciers in Kangri Karpo Mountain is
12 situated at around 4852 m, 5215 m for glaciers on the north slope and 4639 m on the south. This is
13 consistent with the tendency of equilibrium line altitude in southeast Tibetan Plateau (Su et al.,
14 2014). The mean glacier surface slope in the Kangri Karpo Mountain is 24.1° ; with most in the
15 $12^\circ\text{-}32^\circ$ range that accounts for 80.5% of the glaciers and 85.4% of their area. Most glaciers have a
16 SE, S or SW aspects, account for 59.2% and 80.9% of glacier number and area, respectively.

17 Comparing the total area of all glaciers in 1980 with that in 2015, ice cover in the Kangri
18 Karpo Mountain diminished by $679.51 \pm 59.49 \text{ km}^2$ ($24.9\% \pm 2.2\%$) or $0.71\% \pm 0.06\% \text{ a}^{-1}$. Small
19 glaciers shrunk in area in larger percentage (Fig. 5C). Meanwhile, absolute area loss was higher
20 for larger glaciers. Analysis of the glacier hypsography indicated that ice coverage disappeared
21 completely below 2500 m, the highest absolute area loss occurred in the 4500 – 4700 m a.s.l.
22 altitude range, and ice coverage remains almost unchanged above 5800 m. The average minimum
23 elevation of the glaciers increased by 106 m, while median elevation rose about 56 m from 4796
24 to 4852 m.

25 There was a slight tendency that the rate of glaciers shrinkage from 1980 – 2000 was lower
26 than those from 2000 – 2015 in the detailed study area of Kangri Karpo Mountain (Table 3). In the
27 period of 1980 – 2000, glacier area decreased by $63.72 \pm 9.06 \text{ km}^2$ from its original 784.60 km^2
28 ($8.1\% \pm 1.2\%$) or $0.41\% \pm 0.06\% \text{ a}^{-1}$. Between 2000 and 2015, glaciers experienced a reduction of
29 $56.00 \pm 10.97 \text{ km}^2$ ($7.8\% \pm 1.5\%$) or $0.52\% \pm 0.10\% \text{ a}^{-1}$. A detailed analysis of ten sample glaciers
30 confirmed that all glaciers decreased continuously throughout all investigated periods (Table 4).
31 Percentage area loss varied between 8.6% (WGI ID/GLIMS ID: 5O291B0200/G097005E29155N,
32 the smallest glacier loss) and 20.9% (Parlung No. 10 Glacier, the largest one) from 1980 – 2015.
33 While the largest loss of absolute area reached 20.43 km^2 for Yalong Glacier, and lowest reached
34 1.04 km^2 for Parlung No. 10 Glacier.

35 5.2 Length change

36 Comparing the terminal of all glaciers, only nine glaciers advanced while others retreated in the
37 Kangri Karpo Mountain from 1980 – 2015. The nine glaciers experienced a mean advance of 14.8
38 m a^{-1} , and the length of centerlines increased between 103 m and 1547 m. The terminus elevation
39 decrease of these advanced glaciers averaged at 191 m, varying between 34 m (the smallest
40 lowering from 4796 m to 4762 m a.s.l. altitude) and 412 m (the largest one from 4362 m to 3949
41 m a.s.l. altitude) (Table 5). Based on different glacier size, slope and aspect, 86 glaciers were
42 selected from all retreated glaciers to analyze the changes of length. These selected glaciers
43 experienced a mean recession of 759 m (21.7 m a^{-1}) with smallest of 6 m and largest of 3956 m.



1 Similar to area change of the glaciers in the case study region, these glaciers have shown
2 accelerated retreat during the two periods from 1980 – 2000 and from 2000 – 2015 as measured in
3 glacier length (Table 6). Glaciers experienced a mean length reduction of 21.0 m a^{-1} (varying from
4 2.5 m a^{-1} to 104.2 m a^{-1}) in the period of 1980 – 2000 and 22.6 m a^{-1} from 2000 – 2015 (varied
5 between 1.3 m a^{-1} and 144.8 m a^{-1}). The recession of Yalong Glacier changed from 78.0 m a^{-1} in
6 1980 – 2000 to 13.6 m a^{-1} in 2000-2014, while the average rates of retreat increased significantly
7 for Azha Glacier in the two sub-periods of 1980 – 2000 and 2000 – 2015, with a mean recession of
8 11.3 m a^{-1} and 144.8 m a^{-1} , respectively.

9 **5.3 Mass balance**

10 The average elevation change of the entire glacier surfaces in the case study area of Kangri Karpo
11 Mountain was $-17.46 \pm 0.54 \text{ m}$ from 1980-2014. The glaciers, with an area of 788.28 km^2 , have
12 experienced a mean thinning of $0.51 \pm 0.09 \text{ m a}^{-1}$, or mean mass deficit of $0.46 \pm 0.08 \text{ m w.e. a}^{-1}$,
13 equivalent to an overall mass change of $-13.76 \pm 0.43 \text{ Gt}$ for the case study area during 1980-2014.
14 Thinning of these glaciers has speeded up during the periods of 1980-2000 and 2000-2014. From
15 1980-2000, glaciers have thinned by $5.30 \pm 0.77 \text{ m}$ on average, and experienced a mass loss of
16 $0.24 \pm 0.16 \text{ m w.e. a}^{-1}$. Then a surface lowering of $11.04 \pm 0.43 \text{ m}$ was found from 2000-2014,
17 with a mass loss of $0.71 \pm 0.10 \text{ m w.e. a}^{-1}$ (Fig. 6 and Table 7).

18 Heterogeneous glacier mass balance was presented in the detailed study area of Kangri Karpo
19 Mountain during 1980-2014. Glaciers, with an area of $471.05 \pm 3.03 \text{ km}^2$ in the drainage basin of
20 5O282B, experienced greater mass deficit of $0.51 \pm 0.22 \text{ m w.e. a}^{-1}$ from 1980-2014, and mean
21 mass loss of $0.30 \pm 0.14 \text{ m w.e. a}^{-1}$ and $0.76 \pm 0.22 \text{ m w.e. a}^{-1}$ during the periods of 1980-2000 and
22 2000-2014, respectively. Mean mass deficit of $0.39 \pm 0.11 \text{ m w.e. a}^{-1}$ in the drainage basin of
23 5O291B was smaller than those in 5O282B drainage basin during 1980-2014. Glaciers with an
24 area of $317.22 \pm 4.27 \text{ km}^2$ in 5O291B drainage basin experienced accelerating mass loss during
25 the periods of 1980-2000 and 2000-2014, with mean mass loss of $0.13 \pm 0.16 \text{ m w.e. a}^{-1}$ and 0.63
26 $\pm 0.04 \text{ m w.e. a}^{-1}$.

27 Ablation area and accumulation area both experienced mass loss in the detailed study area of
28 Kangri Karpo Mountain from 1980-2014, with mean mass loss of $0.73 \pm 0.08 \text{ m w.e. a}^{-1}$ and 0.32
29 $\pm 0.08 \text{ m w.e. a}^{-1}$, respectively. Glaciers in ablation area experienced accelerating mass loss from
30 1980-2014, while the rate of mass loss remain stable in accumulation area during the whole period.
31 The latter period since 2000 has seen a mass loss of $1.35 \pm 0.04 \text{ m w.e. a}^{-1}$, almost 4 folds ($0.27 \pm$
32 $0.16 \text{ m w.e. a}^{-1}$) before 2000. Mass losses in accumulation area were similar during 1980-2000 and
33 2000-2014, with values of $0.22 \pm 0.14 \text{ m w.e. a}^{-1}$ and $0.37 \pm 0.22 \text{ m w.e. a}^{-1}$.

34 Prominent thickening (elevation increase) was found on the termini of two glaciers on the
35 southern slope of the Kangri Karpo Mountain (Fig. 6C, WGI: 5O291B0113 and 5O291B0117).
36 Probably the effect of debris cover, the glacier terminus of 5O291B0113 and 5O291B0117
37 remains stable between October 1980 and October 2015.

38 **6 Discussion**

39 **6.1 Uncertainty**

40 The uncertainty of glacier outlines was caused by positional and processing errors associated
41 with glacier delineation (Bolch et al., 2010a; Racoviteanu et al., 2009). Seasonal snow, cloud and
42 debris cover complicated glacier mapping precisely (Paul et al., 2013). The accuracy of glacier
43 outlines in this study was estimated by compare extracted results with independently digitized



1 glacier outlines from high resolution aerial imagery at random locations. An uncertainty model
2 was employed to assess accuracy estimated in this study (Pfeffer et al., 2014). The delineation
3 uncertainty of glaciers in the Kangri Karpo Mountain in 2015 was about 24.33 km² using the
4 uncertainty model, that is smaller than the uncertainty of 48.65 km² in this study. Main reason for
5 this discrepancy is probably that the delineation uncertainty of glaciers have been overestimated in
6 this study, especially in the area of debris-covered ice and exposed bedrock that surrounded by ice
7 cover.

8 For the uncertainty of mass balance, the penetration depth of SRTM C-band radar beam into
9 snow and ice was critical issue when SRTM DEM was employed for geodetic mass balance
10 calculations. The penetration depth of SRTM C-band radar beam can be estimated by comparing
11 the SRTM C-band with the SRTM X-band DEM (Gardelle et al., 2012a; Kääb et al., 2012).
12 Previous studies indicated that the penetration depth decreases as temperature and water content of
13 surface snow cover rise (Surdyk, 2002), and penetration depths at 10 GHz from 2.1 m to 4.7 m
14 were measured in Antarctica (Davis and Poznyak, 1993). Glaciers in eastern Nyainqentanglha
15 Mountain are predominantly monsoonal influenced and have more snow moisture and higher
16 temperatures than the Antarctic ice sheet (Shi and Liu, 2000). Hence, the penetration correction is
17 suitable under the assumption that the influence of slight penetration of the X-band is negligible.
18 The mean SRTM C-band penetration was 1.24 m in Kangri Karpo Mountain, led to mass changes
19 on average of +0.06 m w.e. a⁻¹ and -0.08 m w.e. a⁻¹ for the periods of 1980-2000 and 2000-2014.

20 Another issue is the lack of information in several regions due to data voids in accumulation
21 area. Different suitable assumptions or elevation changes in the accumulation regions were used to
22 fill the data voids and to assess the impact on mass balance (Pieczonka et al., 2013; Shangguan
23 et al., 2015). In this study, the information of elevation change exists in all altitudinal zones from
24 2400 m to 6600 m a.s.l., and the area of data voids was too small (0.7% above 6000 m a.s.l. in
25 area) to affect the mass balance significantly. Hence, data voids can be neglected when mass
26 balance was estimated by all glaciers area in the detailed study area, average surface elevation
27 change and ice density.

28 6.2 Glacier change of area and length

29 This study found glacier shrinkage in Kangri Karpo Mountain between 1980 and 2014 of
30 about 0.71% ± 0.06% a⁻¹. In the period of 1980 – 2000, glacier area decreased by 0.41% ± 0.06%
31 a⁻¹ in the case study area, and then this value increased to 0.52% ± 0.10% a⁻¹ after 2000. Our result
32 is in agreement with previous study, that found shrinkage of 0.57% a⁻¹ in the southeastern Tibetan
33 Plateau from 1980-2001 (Yao et al., 2012a). The shrinkage rate of previous study is larger than our
34 result slightly, main reason for that is probably the difference of glacier size. The mean glacier
35 sizes are about 2.07 km² and 6.54 km² in the Kangri Karpo Mountain and in the detailed study
36 area in 1980, and greater relative loss for smaller glaciers was found in this study and previous
37 studies (Wei et al., 2014; Wu et al., 2016b).

38 Compared with the retreat of mountain glaciers in the western China, glaciers in Kangri
39 Karpo Mountain have experienced extremely strong glacial retreat. The glacier retreat of about
40 0.71% a⁻¹ is lower than that in Altay Mountain (0.75% a⁻¹) (Yao et al., 2012b), but larger than that
41 in other regions of western China, such as Tian Shan Mountains (0.22% a⁻¹) (Wang et al., 2011),
42 eastern Pamir (0.25% a⁻¹) (Zhang et al., 2016b), western Kunlun Mountain (0.09% a⁻¹) (Bao et al.,
43 2015), Qilian Mountain (0.47% a⁻¹) (Sun et al., 2015), Tibetan Plateau interior area (0.26% a⁻¹)
44 (Wei et al., 2014).



1 The location of glacier terminal is often measured by remote sensing and investigation in the
2 field. Due to the differences in the periods studied and spatial scales, the length changes of glacier
3 centerlines in this study are slower than previous studies, except for Azha Glacier (Liu et al., 2006;
4 Yang et al., 2010; Yao et al., 2012a). The investigation of terminus variation on Parlung No. 10
5 Glacier was surveyed from 2006-2008, the period of survey is too short to represent length change
6 of glacier centerlines over long periods of time (Yang et al., 2010). Compared the length change of
7 Azha Glacier in different periods, -56.1 m a^{-1} from 1973-2005 (Yao et al., 2012a), -65 m a^{-1} from
8 1980-2006 (Yang et al., 2010) and -70 m a^{-1} from 1980-2015 (this study), we can found that Azha
9 Glacier have experienced greater retreat after 2000s than that before 2000s. The length change of
10 Yalong Glacier from 1980-2000 in this study is similar with Liu et al. (Liu et al., 2006), who
11 found retreat of 73 m a^{-1} of Yalong Glacier between 1980 and 2001. And then the average rate of
12 retreat decreased significantly for Yalong Glacier after 2000. Main reason is probably that flow
13 velocity increased and more ice and snow are transported from accumulation area to glacier
14 terminal.

15 For advanced glaciers, the mean glacier size is about 0.51 km^2 and mean glacier surface slope
16 is about 27.9° ; most glaciers have an S or SW aspect, and mean accumulation area ratio (AAR) is
17 51. Previous studies also found advanced glaciers in Kangri Karpo Mountain (Liu et al., 2006; Shi
18 et al., 2006). Compared with the CGI2 and GAMDAM glacier inventory, the location of most
19 glacier terminals in 2000 and 2014 are closed, indicated that glacier advancing mainly occurs
20 before 2000. This behavior may be related to the increase of high precipitation (Shi et al., 2006),
21 or a phenomenon of glacier surging, and requires further investigation.

22 6.3 Glacier thinning and mass balance

23 A comparison of glacier thickness changes show that significant differences are found over
24 eastern Nyainqentanglha Mountain. Using SRTM DEM and SPOT5 DEM (24 November 2011),
25 glaciers experienced a mean thinning of $0.39 \pm 0.16 \text{ m a}^{-1}$ in eastern Nyainqentanglha Mountains
26 (named Hengduan Shan) (Gardelle et al., 2013). Based on ICESat and SRTM, (Kääb et al., 2015),
27 (Neckel et al., 2014) and (Gardner et al., 2013) acquired different results over eastern
28 Nyainqentanglha Mountain, with glacier thickness loss of $1.34 \pm 0.29 \text{ m a}^{-1}$, $0.81 \pm 0.32 \text{ m a}^{-1}$ and
29 $0.30 \pm 0.13 \text{ m a}^{-1}$, respectively. Using SRTM DEM and TerraSAR-X/TanDEM-X acquisitions (18
30 February 2014 and 13 March 2014), glaciers experienced a mean thinning of $0.79 \pm 0.11 \text{ m a}^{-1}$ in
31 Kangri Karpo Mountain. At a first glance, the result of glacier thickness loss in this study is in
32 agreement with (Neckel et al., 2014), and have significant differences with (Kääb et al., 2015).
33 Main reason for this discrepancy is the different estimation of SRTM C-band penetration. An
34 average SRTM C-band penetration of 1.24 m was used for Kangri Karpo Mountain that estimated
35 from the difference of SRTM C-band and X-band DEMs (Gardelle et al., 2012a). While an
36 average penetration of 8-10 m (7-9 m if based on the winter trends that might alternatively be
37 assumed to reflect February conditions) was employed for eastern Nyainqentanglha Mountain
38 (Kääb et al., 2015). Previous studies indicated that the penetration depth varies with temperature
39 and water content (Surdyk, 2002), and penetration depths of SRTM C-band from 1.4 m to 3.4 m
40 were estimated over the Pamir-Karakoram-Himalaya (Gardelle et al., 2013; Kääb et al., 2012).
41 The characteristics of glaciers in eastern Nyainqentanglha Mountain are similar with that in
42 eastern Himalaya (Shi et al., 2008b). Therefore, the penetration in this study is more suitable
43 under the assumption that the penetrations in eastern Nyainqentanglha Mountain and eastern
44 Himalaya are similar.



1 Field measurement of mass balance is the best indicator of glacier change. A monitoring
2 program has been carried out on Parlung No. 4 Glacier (5O282B0004/G096920E29228N) and
3 Parlung No. 10 Glacier (5O282B0010/G096904E29286N), both located on the northern slope of
4 the Kangri Karpo Mountain. Large ice deficit were found on the two monitored glaciers at rates of
5 $-0.71 \text{ m w.e. a}^{-1}$ from May 2006 to May 2007 and $-0.78 \text{ m w.e. a}^{-1}$ during 2005-2009, respectively
6 (Yang et al., 2008; Yao et al., 2012a). Based on SRTM DEM and TerraSAR-X/TanDEM-X
7 acquisitions (18 February 2014), the two glaciers experienced large surface lowering from 2000 to
8 2014, with mean mass loss of $0.65 \pm 0.22 \text{ m w.e. a}^{-1}$ and $0.67 \pm 0.22 \text{ m w.e. a}^{-1}$. The comparison
9 between filed measurements of mass balance and the result of this study indicated that there was
10 high consistency of glacier mass loss about Parlung No. 4 Glacier and Parlung No. 10 Glacier.

11 Interestingly is the bigger thinning on the debris-covered regions of $-0.99 \pm 0.09 \text{ m a}^{-1}$ on
12 average than clean-ice region of $-0.89 \pm 0.08 \text{ m w.e. a}^{-1}$ from 1980-2014 (Fig. 7). Due to complex
13 surface conditions, such as supraglacial lakes, ice cliffs and heterogeneity of debris cover, the
14 mass loss patterns on the debris-covered tongue are complicated (Pellicciotti et al., 2015). It is
15 generally believed that ice ablation rate is highly reduced with the thick debris-cover due to the
16 insulation effect of debris. However, previous studies found that glacier ablation on debris-covered
17 regions were greater than on the exposed ice regions (Pu et al., 2003; Ye et al., 2015; Zhang et al.,
18 2016a). The location of debris-covered regions, in the lower altitudes with higher temperature, and
19 the development of supraglacial lakes and ice cliffs are probably the reasons for the larger mass
20 loss on the debris-covered regions (Benn et al., 2012; Sakai and Fujita, 2010).

21 Overall, negative elevation changes were found in glacier tongue regions except for two
22 glaciers in the southern slope of the Kangri Karpo Mountain (Fig. 6C). Compared the average
23 elevation changes of the two glaciers tongue surface during 1980-2000 and 2000-2014, positive
24 elevation changes were found between October 1980 and February 2000, and negative elevation
25 changes were found after 2000. The two glaciers showed positive elevation changes at the
26 terminuses, while elevation changes are unknown in accumulation area of the two glaciers due to
27 data voids. This phenomenon could be interpreted as glacier surging (Cuffey and Paterson, 2010),
28 or result from the increase of high precipitation (Shi et al., 2006).

29 **6.4 Climatic considerations**

30 The climate in Kangri Karpo Mountain is characterized be the westerly in winter and the
31 Indian monsoon in summer (Li et al., 1986). While the effects of westerly are weak in the study
32 area due to the block of Tibetan Plateau. Hence, the accumulation on glaciers in Kangri Karpo
33 Mountain is supplied by summer monsoon precipitation (Bolch et al., 2010a; Yao et al., 2012a).
34 Previous studies indicated that the Tibetan Plateau has experienced an overall surface air warming
35 since the mid-1950s (Duan et al., 2015; Li et al., 2010; Liu et al., 2008; Liu et al., 2009; Qin et al.,
36 2009; Yang et al., 2014; Yao et al., 2012a; You et al., 2010). Different trend of average annual
37 temperature results from different data in the southeastern TP. Based on temperature data from
38 meteorological stations, the southeastern TP present the lowest warming rate (Duan et al., 2015),
39 while the most warming rate was found from the MODIS land surface temperature (MODIS LST)
40 in the southeastern TP (Yang et al., 2014), even decreasing trend of average annual temperature
41 was found from the National Centers for Environmental Prediction/National Center for
42 Atmospheric Research (NCEP/NCAR) Reanalysis data (You et al., 2010). The changes in air
43 temperature were accompanied by the changes in precipitation due to variations in monsoonal
44 activity. Based on the Global Precipitation Climatology Project (GPCP) data, precipitation



1 decreased in the southeastern TP from 1979 to 2010 (Yao et al., 2012a). While positive trend of
2 annual precipitation was found from Chinese meteorological stations data in the southeastern TP,
3 precipitation amount increased and the frequency of severely dry events decreased significantly
4 (Li et al., 2010). Due to the ambiguous of climate change, the presented glacier changes and mass
5 balance cannot be explained by the above summarized climate variations directly.

6 In order to analyze the response of glaciers to climate change, air temperature and
7 precipitation datasets were collected from the China Meteorological Forcing Dataset (CMFD,
8 1979.01.01 – 2012.12.31) (Chen et al., 2011; He and Yang, 2011), which produced by merging a
9 variety of data sources, including meteorological station data, TRMM satellite precipitation
10 analysis data, GEWEX-SRB downward shortwave radiation data and GLDAS data
11 (<http://westdc.westgis.ac.cn/data/7a35329c-c53f-4267-aa07-e0037d913a21>). The horizontal
12 distributions of surface temperature change and precipitation change from May to September
13 derived from the CMFD data was shown in Fig. 8. It is clear that warming is a dominant
14 phenomenon in the southeastern TP during recent decades. The warming rate on the northern
15 slope of the Kangri Karpo Mountain is larger than that on the southern slope slightly. The law of
16 precipitation change was inconsistent that an increasing trend was present in much of Kangri
17 Karpo Mountain, but a decreasing trend in the eastern Kangri Karpo Mountain. The changes of air
18 temperature and precipitation are confirmed by three nearest meteorological stations datasets,
19 which is Bomi (2736 m a.s.l.), Zuogong (3780 m a.s.l.) and Zayu (2423 m a.s.l.) (Liu et al., 2006;
20 Yang et al., 2010). The air temperature at the three meteorological stations increased slightly from
21 1980-2000, and then it increased significantly after 2000. Despite large inter-annual fluctuation of
22 precipitation, statistically significant trends are not evident at the three stations (Wu et al., 2016a;
23 Yang et al., 2010). Hence, glaciers change in the Kangri Karpo Mountain can be attributed to
24 climate warming, especially the rate of glaciers shrinkage and mass loss from 1980 – 2000 were
25 lower than those from 2000 – 2015, and mean mass deficit in northern slope was larger than those
26 in southern slope during 1980-2014, which is consistent with the tendency of climate warming.

27 7 Conclusions

28 This study estimated glacier area, glacier length, surface elevation and mass balance of the Kangri
29 Karpo Mountain for the period of 1980-2015 based on Topographic Maps, Landsat images, SRTM
30 and TerraSAR-X/TanDEM-X acquisitions.

31 Our results show that the Kangri Karpo Mountain contains 1166 glaciers, with an area of
32 $2048.50 \pm 48.65 \text{ km}^2$ in 2015. Ice cover in the Kangri Karpo Mountain diminished by $679.51 \pm$
33 59.49 km^2 ($24.9\% \pm 2.2\%$) or $0.71\% \pm 0.06\% \text{ a}^{-1}$ from 1980-2015. Comparing the terminal of all
34 glaciers, only nine glaciers advanced while others retreated in the Kangri Karpo Mountain from
35 1980 – 2015. Compared with the retreat of mountain glaciers in the western China, glaciers in
36 Kangri Karpo Mountain have experienced extremely strong glacial retreat.

37 The average elevation change of the entire glacier surfaces in the detailed study area of
38 Kangri Karpo Mountain was $-0.51 \pm 0.09 \text{ m a}^{-1}$, or mean mass deficit of $0.46 \pm 0.08 \text{ m w.e. a}^{-1}$
39 from 1980-2014. Heterogeneous glacier mass balance was presented in the Kangri Karpo
40 Mountain during 1980-2014. The comparison between filed measurements of mass balance and
41 the result of this study indicated that there was high consistency of glacier mass loss about Parlung
42 No. 4 Glacier and Parlung No. 10 Glacier. Geodetic mass balance measurements in the detailed
43 study area of Kangri Karpo Mountain revealed that the debris-covered regions exhibit higher
44 thinning rates than the clean-ice region on average obviously, with an average of $-0.99 \pm 0.09 \text{ m}$



1 a^{-1} ($-0.89 \pm 0.08 \text{ m w.e. a}^{-1}$) from 1980-2014. There was a slight tendency that the rate of glaciers
2 shrinkage and mass loss from 1980 – 2000 were lower than those from 2000 – 2015 in the detailed
3 study area of Kangri Karpo Mountain.

4
5
6
7 *Acknowledgements.* This work was supported by the fundamental program from the Ministry of Science and
8 Technology of China (MOST) (Grant No. 2013FY111400), the National Natural Science Foundation of China
9 (Grant No. 41190084) and the International Partnership Program of Chinese Academy of Sciences (Grant No.
10 131C11KY5B20160061). Landsat images are from the U. S. Geological Survey and NASA. The GAMDAM
11 glacier inventory is from Dr. A. Sakai . The first and second glacier inventories were provided by an
12 immediate past MOST project (2006FY110200). The China Meteorological Forcing Dataset (CMFD) is
13 from Cold and Arid Regions Science Data Center at Lanzhou. All SAR processing was done with the GAMMA
14 SAR and interferometric processing software.

17 18 **References**

- 19
20 Arendt, A., Bliss, A., Bolch, T., Cogley, J. G., and Gardner, A. S.: Randolph Glacier Inventory - A
21 dataset of global glacier outlines: Version 5.0. University of Colorado, National Snow and Ice Data
22 Center (NSIDC), Global Land Ice Measurements from Space (GLIMS), Boulder, CO, USA. Available
23 online at: http://www.glims.org/RGI/00_rgi50_TechnicalNote.pdf, 2015.
- 24 Bao, W., Liu, S., Wei, J., and Guo, W.: Glacier changes during the past 40 years in the West Kunlun
25 Shan, *Journal of Mountain Science*, 12, 344-357, 2015.
- 26 Benn, D. I., Bolch, T., Hands, K., Gulley, J., Luckman, A., Nicholson, L. I., Quincey, D., Thompson, S.,
27 Toumi, R., and Wiseman, S.: Response of debris-covered glaciers in the Mount Everest region to recent
28 warming, and implications for outburst flood hazards, *Earth-Science Reviews*, 114, 156-174, 2012.
- 29 Berthier, E., Arnaud, Y., Vincent, C., and Remy, F.: Biases of SRTM in high - mountain areas:
30 Implications for the monitoring of glacier volume changes, *Geophysical Research Letters*, 33, 2006.
- 31 Berthier, E., Schiefer, E., Clarke, G. K., Menounos, B., and Rány, F.: Contribution of Alaskan glaciers
32 to sea-level rise derived from satellite imagery, *Nature Geoscience*, 3, 92-95, 2010.
- 33 Bolch, T., Menounos, B., and Wheate, R.: Landsat-based inventory of glaciers in western Canada,
34 1985–2005, *Remote Sensing of Environment*, 114, 127-137, 2010a.
- 35 Bolch, T., Pieczonka, T., and Benn, D.: Multi-decadal mass loss of glaciers in the Everest area (Nepal
36 Himalaya) derived from stereo imagery, *The Cryosphere*, 5, 349-358, 2011.
- 37 Bolch, T., Yao, T., Kang, S., Buchroithner, M., Scherer, D., Maussion, F., Huintjes, E., and Schneider,
38 C.: A glacier inventory for the western Nyainqentanglha Range and the Nam Co Basin, Tibet, and
39 glacier changes 1976–2009, *The Cryosphere*, 4, 419-433, 2010b.
- 40 Chen, Y., Yang, K., He, J., Qin, J., Shi, J., Du, J., and He, Q.: Improving land surface temperature
41 modeling for dry land of China, *Journal of Geophysical Research Atmospheres*, 116, 999-1010, 2011.
- 42 Cuffey, K. M. and Paterson, W. S. B.: *The Physics of Glaciers* (Fourth Edition),
43 Butterworth-Heinemann/Elsevier, Burlington, MA, USA and Oxford, UK, 2010.
- 44 Dall, J., Madsen, S. N., Keller, K., and Forsberg, R.: Topography and penetration of the Greenland ice



- 1 sheet measured with airborne SAR interferometry, *Geophysical Research Letters*, 28, 1703-1706, 2001.
- 2 Davis, C. H. and Poznyak, V. I.: The depth of penetration in Antarctic firn at 10 GHz, *IEEE*
- 3 *Transactions on Geoscience & Remote Sensing*, 31, 1107-1111, 1993.
- 4 Duan, J., Li, L., and Fang, Y.: Seasonal spatial heterogeneity of warming rates on the Tibetan Plateau
- 5 over the past 30 years, *Scientific Reports*, 5, 2015.
- 6 Farr, T. G., Rosen, P. A., Caro, E., Crippen, R., Duren, R., Hensley, S., Kobrick, M., Paller, M.,
- 7 Rodriguez, E., Roth, L., Seal, D., Shaffer, S., Shimada, J., Umland, J., Werner, M., Oskin, M., Burbank,
- 8 D., and Alsdorf, D.: The shuttle radar topography mission, *Reviews of geophysics*, 45, 2007.
- 9 Gardelle, J., Berthier, E., and Arnaud, Y.: Impact of resolution and radar penetration on glacier
- 10 elevation changes computed from DEM differencing, *Journal of Glaciology*, 58, 419-422, 2012a.
- 11 Gardelle, J., Berthier, E., and Arnaud, Y.: Slight mass gain of Karakoram glaciers in the early
- 12 twenty-first century, *Nature geoscience*, 5, 322-325, 2012b.
- 13 Gardelle, J., Berthier, E., Arnaud, Y., and Kaab, A.: Region-wide glacier mass balances over the
- 14 Pamir-Karakoram-Himalaya during 1999-2011, *Cryosphere*, 7, 1885-1886, 2013.
- 15 Gardner, A. S., Moholdt, G., Cogley, J. G., Wouters, B., Arendt, A. A., Wahr, J., Berthier, E., Hock, R.,
- 16 Pfeffer, W. T., and Kaser, G.: A reconciled estimate of glacier contributions to sea level rise: 2003 to
- 17 2009, *Science*, 340, 852-857, 2013.
- 18 GB/T12343.1: Compilation specifications for national fundamental scale maps —Part 1: compilation
- 19 specifications for 1:25000/1:50000/1:100000 topographic maps., General Administration of Quality
- 20 Supervision, Inspection and Quarantine, Beijing, 2008.
- 21 Goldstein, R. M. and Werner, C. L.: Radar interferogram filtering for geophysical applications,
- 22 *Geophysical Research Letters*, 25, 4035-4038, 1998.
- 23 Guo, W., Liu, S., Xu, J., Wu, L., Shanguan, D., Yao, X., Wei, J., Bao, W., Yu, P., and Liu, Q.: The
- 24 second Chinese glacier inventory: data, methods and results, *Journal of Glaciology*, 61, 357-372, 2015.
- 25 Guo, W., Liu, S., Yu, P., and Xu, J.: Automatic extraction of ridgelines using on drainage boundaries
- 26 and aspect difference, *Science of Surveying and Mapping*, 36, 210-213, 2011.
- 27 He, J. and Yang, K.: China Meteorological Forcing Dataset. Center, C. a. A. R. S. D., Lanzhou, 2011.
- 28 Immerzeel, W. W., Van Beek, L. P., and Bierkens, M. F.: Climate change will affect the Asian water
- 29 towers, *Science*, 328, 1382-1385, 2010.
- 30 IPCC: Summary for policymakers. In: *Climate change 2013: The physical science basis. Contribution*
- 31 *of Working Group I to the Fifth Assessment Report of the Intergovernmental Panel on Climate*
- 32 *Change.*, Cambridge University Press Cambridge, UK and New York, NY, USA, 2013.
- 33 Kääb, A., Berthier, E., Nuth, C., Gardelle, J., and Arnaud, Y.: Contrasting patterns of early
- 34 twenty-first-century glacier mass change in the Himalayas, *Nature*, 488, 495-498, 2012.
- 35 Kääb, A., Treichler, D., Nuth, C., and Berthier, E.: Brief Communication: Contending estimates of
- 36 2003–2008 glacier mass balance over the Pamir–Karakoram–Himalaya, *The Cryosphere*, 9, 557-564,
- 37 2015.
- 38 Kienholz, C., Rich, J., Arendt, A., and Hock, R.: A new method for deriving glacier centerlines applied
- 39 to glaciers in Alaska and northwest Canada, *The Cryosphere*, 8, 503-519, 2014.
- 40 Koblet, T., GärtnerRoer, I., Zemp, M., and Jansson, P.: Reanalysis of multi-temporal aerial images of
- 41 Storglaciären, Sweden (1959–99) – Part 1: Determination of length, area, and volume changes,
- 42 *Cryosphere*, 4, 333-343, 2010.
- 43 Krieger, G., Moreira, A., Fiedler, H., and Hajnsek, I.: TanDEM-X: A Satellite Formation for
- 44 High-Resolution SAR Interferometry, *Geoscience and Remote Sensing, IEEE Transactions on*, 45,



- 1 3317-3341, 2007.
- 2 Le Bris, R. and Paul, F.: An automatic method to create flow lines for determination of glacier length: A
- 3 pilot study with Alaskan glaciers, *Computers & Geosciences*, 52, 234-245, 2013.
- 4 Leclercq, P. W., Oerlemans, J., Basagic, H. J., Bushueva, I., Cook, A., and Le Bris, R.: A data set of
- 5 worldwide glacier length fluctuations, *The Cryosphere*, 8, 659-672, 2014.
- 6 Li, J., Zhen, B., and Yang, X.: *The glaciers of Xizang (Tibet)*, Science Press, Chinese Academy of
- 7 Sciences, Beijing, 1986.
- 8 Li, L., Yang, S., Wang, Z., Zhu, X., and Tang, H.: Evidence of warming and wetting climate over the
- 9 Qinghai-Tibet Plateau, *Arctic Antarctic & Alpine Research*, 42, 449-457, 2010.
- 10 Li, X., Cheng, G., Jin, H., Kang, E., Che, T., Jin, R., Wu, L., Nan, Z., Wang, J., and Shen, Y.:
- 11 Cryospheric change in China, *Global and Planetary Change*, 62, 210-218, 2008.
- 12 Li, X., Yang, T., and Ji, Q.: Study on Glacier Variations in the Gangrigabu Range, *Research of Soil and*
- 13 *Water Conservation*, 21, 233-237, 2014.
- 14 Liu, S., Shangguan, D., Ding, Y., Han, H., Xie, C., Zhang, Y., Li, J., Wang, J., and Li, G.: Glacier
- 15 changes during the past century in the Gangrigabu mountains, southeast Qinghai–Xizang (Tibetan)
- 16 Plateau, China, *Annals of Glaciology*, 43, 187-193, 2006.
- 17 Liu, W., Guo, Q., and Wang, Y.: Temporal-spatial climate change in the last 35 years in Tibet and its
- 18 geo-environmental consequences, *Environmental geology*, 54, 1747-1754, 2008.
- 19 Liu, X., Cheng, Z., Yan, L., and Yin, Z.-Y.: Elevation dependency of recent and future minimum
- 20 surface air temperature trends in the Tibetan Plateau and its surroundings, *Global and Planetary Change*,
- 21 68, 164-174, 2009.
- 22 Mi, D., Xie, Z., Luo, R., and Feng, Q.: *Glacier inventory of China XI. The Ganga Drainage basin*. ,
- 23 Xi'an Cartographic Publishing House, Xi'an, 2002.
- 24 Neckel, N., Braun, A., Kropáček, J., and Hochschild, V.: Recent mass balance of Purogangri ice cap,
- 25 central Tibetan Plateau, by means of differential X-band SAR interferometry, *Cryosphere*, 7,
- 26 1623-1633, 2013.
- 27 Neckel, N., Kropáček, J., Bolch, T., and Hochschild, V.: Glacier mass changes on the Tibetan Plateau
- 28 2003–2009 derived from ICESat laser altimetry measurements, *Environmental research letters*, 9,
- 29 014009, 2014.
- 30 Nuimura, T., Sakai, A., Taniguchi, K., Nagai, H., Lamsal, D., Tsutaki, S., Kozawa, A., Hoshina, Y.,
- 31 Takenaka, S., and Omiya, S.: The GAMDAM Glacier Inventory: a quality controlled inventory of
- 32 Asian glaciers, *Cryosphere*, 9, 849-864, 2015.
- 33 Nuth, C. and Kääb, A.: Co-registration and bias corrections of satellite elevation data sets for
- 34 quantifying glacier thickness change, *The Cryosphere*, 5, 271-290, 2011.
- 35 Oerlemans, J.: Quantifying global warming from the retreat of glaciers, *Science*, 264, 243-244, 1994.
- 36 Paul, F., Barrand, N. E., Baumann, S., Berthier, E., Bolch, T., Casey, K., Frey, H., Joshi, S. P.,
- 37 Kononov, V., and Bris, R. L.: On the accuracy of glacier outlines derived from remote-sensing data,
- 38 *Annals of Glaciology*, 54, 171-182, 2013.
- 39 Paul, F., Barry, R. G., Cogley, J. G., Frey, H., Haeberli, W., Ohmura, A., Ommanney, C. S. L., Raup, B.,
- 40 Rivera, A., and Zemp, M.: Recommendations for the compilation of glacier inventory data from digital
- 41 sources, *Annals of Glaciology*, 50, 119-126, 2009.
- 42 Paul, F. and Haeberli, W.: Spatial variability of glacier elevation changes in the Swiss Alps obtained
- 43 from two digital elevation models, *Geophysical Research Letters*, 35, 189-203, 2008.
- 44 Paul, F., Kaeab, A., and Maisch, M.: Comparison of TM Derived Glacier Areas With Higher



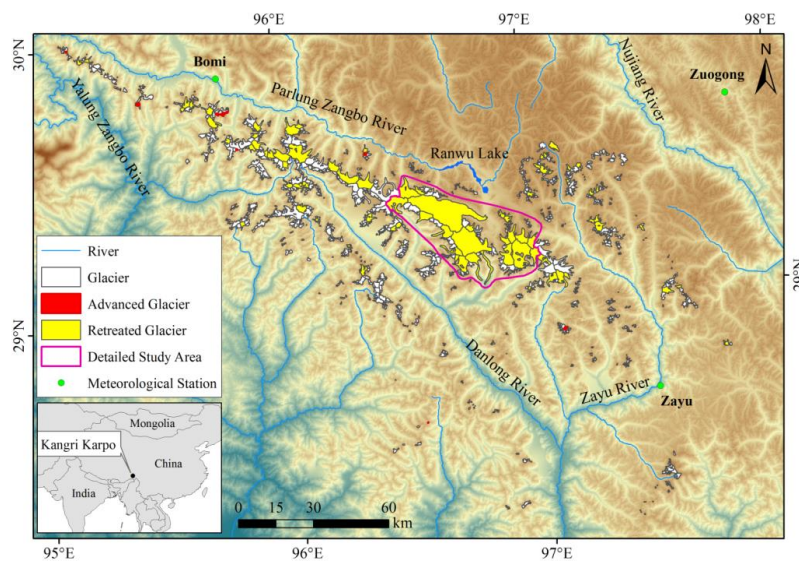
- 1 Resolution Data Sets, *EARSeL eProceedings* 2, 2, 15-21, 2003.
- 2 Paul, F. and Svoboda, F.: A new glacier inventory on southern Baffin Island, Canada, from ASTER data:
- 3 II. Data analysis, glacier change and applications, *Annals of Glaciology*, volume 50, 22-31, 2010.
- 4 Pellicciotti, F., Stephan, C., Miles, E., Herreid, S., Immerzeel, W. W., and Bolch, T.: Mass-balance
- 5 changes of the debris-covered glaciers in the Langtang Himal, Nepal, from 1974 to 1999, *Journal of*
- 6 *Glaciology*, 61, 373-386, 2015.
- 7 Pfeffer, W. T., Arendt, A. A., Bliss, A., Bolch, T., Cogley, J. G., Gardner, A. S., Hagen, J. O., Hock, R.,
- 8 Kaser, G., and Kienholz, C.: The Randolph Glacier Inventory: a globally complete inventory of glaciers,
- 9 *Journal of Glaciology*, 60, 537-552, 2014.
- 10 Pieczonka, T., Tobias, B., Wei, J., and Liu, S.: Heterogeneous mass loss of glaciers in the Aksu-Tarim
- 11 Catchment (Central Tien Shan) revealed by 1976 KH-9 Hexagon and 2009 SPOT-5 stereo imagery,
- 12 *Remote Sensing of Environment*, 130, 233-244, 2013.
- 13 Pu, J., Yao, T., and Duan, K.: An observation on surface ablation on the Yangbark glacier in the
- 14 Muztagata Ata, China, *Journal of Glaciology & Geocryology*, 25, 680-684, 2003.
- 15 Qin, J., Yang, K., Liang, S., and Guo, X.: The altitudinal dependence of recent rapid warming over the
- 16 Tibetan Plateau, *Climatic Change*, 97, 321-327, 2009.
- 17 Rabus, B., Eineder, M., Roth, A., and Bamler, R.: The shuttle radar topography mission—a new class
- 18 of digital elevation models acquired by spaceborne radar, *Isprs Journal of Photogrammetry & Remote*
- 19 *Sensing*, 57, 241-262, 2003.
- 20 Racoviteanu, A. E., Paul, F., Raup, B., Khalsa, S. J. S., and Armstrong, R.: Challenges and
- 21 recommendations in mapping of glacier parameters from space: results of the 2008 Global Land Ice
- 22 Measurements from Space (GLIMS) workshop, Boulder, Colorado, USA, *Annals of Glaciology*, 50,
- 23 53-69, 2009.
- 24 Sakai, A. and Fujita, K.: Formation conditions of supraglacial lakes on debris-covered glaciers in the
- 25 Himalaya, *Journal of Glaciology*, 56, 177-181, 2010.
- 26 Shangguan, D., Liu, S., Ding, Y., Zhang, Y., Li, J., Li, X., and Wu, Z.: Changes in the elevation and
- 27 extent of two glaciers along the Yanglonghe river, Qilian Shan, China, *Journal of Glaciology*, 56,
- 28 309-317, 2010.
- 29 Shangguan, D. H., Bolch, T., Ding, Y. J., Kröhnert, M., Pieczonka, T., Wetzel, H. U., and Liu, S. Y.:
30 Mass changes of Southern and Northern Inylchek Glacier, Central Tian Shan, Kyrgyzstan, during
31 \sim 1975 and 2007 derived from remote sensing data, *Cryosphere*, 9, 703-717, 2015.
- 32 Shi, Y., Huang, M., and Ren, B.: An introduction to the glaciers in China, Science Press, Beijing,
- 33 1988.
- 34 Shi, Y., Huang, M., Yao, T., and He, Y.: *Glaciers and Related Environments in China*, Science Press,
- 35 2008a.
- 36 Shi, Y., Liu, C., Wang, Z., Liu, S., and Ye, B.: *Concise glacier inventory of China*, Shanghai Popular
- 37 Science Press, 2008b.
- 38 Shi, Y. and Liu, S.: Estimation on the response of glaciers in China to the global warming in the 21st
- 39 century, *Chinese Science Bulletin*, 45, 668-672, 2000.
- 40 Shi, Y., Liu, S., Shangguan, D., Li, D., Ye, B., and Shen, Y.: Two peculiar phenomena of climatic and
- 41 glacial variations in the Tibetan Plateau, *Advances in Climate Change Research*, 2, 154-160, 2006.
- 42 Su, Z., Zhao, J., and Zheng, B.: Distribution and features of the glaciers' ELAs and the decrease of
- 43 ELAs during the Last Glaciation in China, *Journal of Glaciology and Geocryology*, 36, 9-19, 2014.
- 44 Sun, M., Liu, S., Yao, X., Guo, W., and Xu, J.: Glacier changes in the Qilian Mountains in the past half



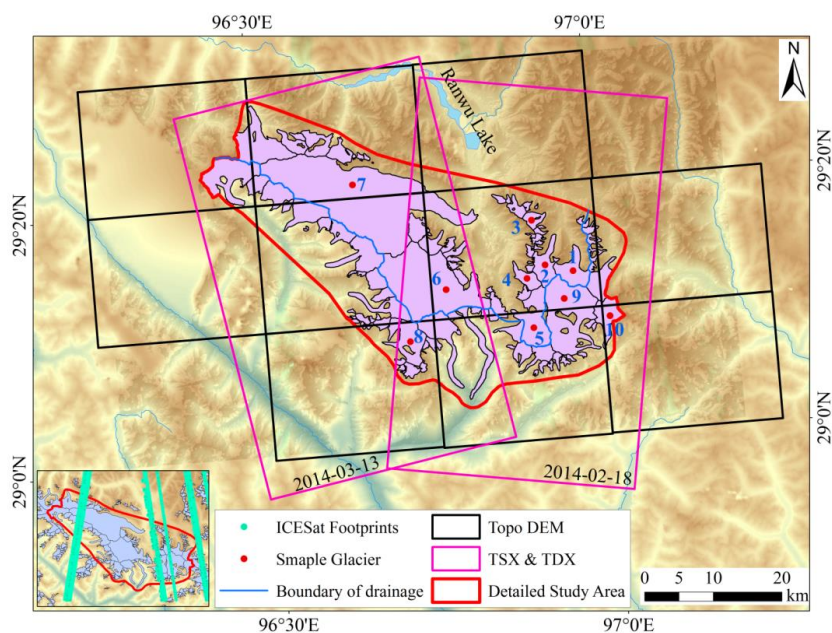
- 1 century: Based on the revised First and Second Chinese Glacier Inventory, ACTA GEOGRAPHICA
2 SINICA, 70, 1402-1414, 2015.
- 3 Surdyk, S.: Using microwave brightness temperature to detect short-term surface air temperature
4 changes in Antarctica: An analytical approach, Remote Sensing of Environment, 80, 256-271, 2002.
- 5 Wang, S., Zhang, M., Li, Z., Wang, F., Li, H., Li, Y., and Huang, X.: Response of glacier area variation
6 to climate change in chinese Tianshan Mountains in the past 50 years, ACTA GEOGRAPHICA
7 SINICA, 66, 38-46, 2011.
- 8 Wei, J., Liu, S., Guo, W., Xu, J., Bao, W., and Shangguan, D.: Changes in glacier volume in the north
9 bank of the Bangong Co Basin from 1968 to 2007 based on historical topographic maps, SRTM, and
10 ASTER stereo images, Arctic, Antarctic, and Alpine Research, 47, 301-311, 2015a.
- 11 Wei, J., Liu, S., Guo, W., Yao, X., Xu, J., Bao, W., and Jiang, Z.: Surface-area changes of glaciers in the
12 Tibetan Plateau interior area since the 1970s using recent Landsat images and historical maps, Annals
13 of Glaciology, 55, 213-222, 2014.
- 14 Wei, J., Liu, S., Xu, J., Guo, W., Bao, W., Shangguan, D., and Jiang, Z.: Mass loss from glaciers in the
15 Chinese Altai Mountains between 1959 and 2008 revealed based on historical maps, SRTM, and
16 ASTER images, Journal of Mountain Science, 12, 330-343, 2015b.
- 17 Werner, C., Wegmüller, U., Strozzi, T., and Wiesmann, A.: Gamma SAR and interferometric processing
18 software, 2000, 1620.
- 19 Wu, K., Liu, S., Bao, W., and Wang, R.: Monitoring Glacier Change Based on Remote Sensing in the
20 Gangrigabu Range, Southeast Tibetan Plateau, From 1980-2015, Journal of Glaciology and
21 Geocryology, 2016a. 2016a.
- 22 Wu, K., Liu, S., Guo, W., Wei, J., Xu, J., Bao, W., and Yao, X.: Glacier change in the western
23 Nyainqentanglha Range, Tibetan Plateau using historical maps and Landsat imagery: 1970-2014,
24 Journal of Mountain Science, 13, 1358-1374, 2016b.
- 25 Xu, J., Liu, S., Zhang, S., Guo, W., and Wang, J.: Recent changes in glacial area and volume on
26 Tuanjiefeng peak region of Qilian Mountains, China, PLoS One, 8, e70574, 2013.
- 27 Yang, K., Wu, H., Qin, J., Lin, C., Tang, W., and Chen, Y.: Recent climate changes over the Tibetan
28 Plateau and their impacts on energy and water cycle: A review, Global & Planetary Change, 112, 79-91,
29 2014.
- 30 Yang, W., Yao, T., Xu, B., Ma, L., Wang, Z., and Wan, M.: Characteristics of recent temperate glacier
31 fluctuations in the Parlung Zangbo River basin, southeast Tibetan Plateau, Chinese Science Bulletin, 55,
32 2097-2102, 2010.
- 33 Yang, W., Yao, T. D., Xu, B. Q., Wu, G. J., Ma, L. L., and Xin, X. D.: Quick ice mass loss and abrupt
34 retreat of the maritime glaciers in the Kangri Karpo Mountains, southeast Tibetan Plateau, Chinese
35 Science Bulletin, 53, 2547-2551, 2008.
- 36 Yao, T., Thompson, L., Yang, W., Yu, W., Gao, Y., Guo, X., Yang, X., Duan, K., Zhao, H., and Xu, B.:
37 Different glacier status with atmospheric circulations in Tibetan Plateau and surroundings, Nature
38 Climate Change, 2, 663-667, 2012a.
- 39 Yao, X., Liu, S., Guo, W., Huai, B., Sun, M., and Xu, J.: Glacier change of Altay Mountain in China
40 from 1960 to 2009--Based on the Second Glacier Inventory of China, Journal of Natural Resources, 27,
41 1734-1745, 2012b.
- 42 Yao, X., Liu, S., zhu, Y., Gong, P., An, L., and Li, X.: Design and implementation of an automatic
43 method for deriving glacier centerlines based on GIS, Journal of Glaciology and Geocryology, 37,
44 1563-1570, 2015.



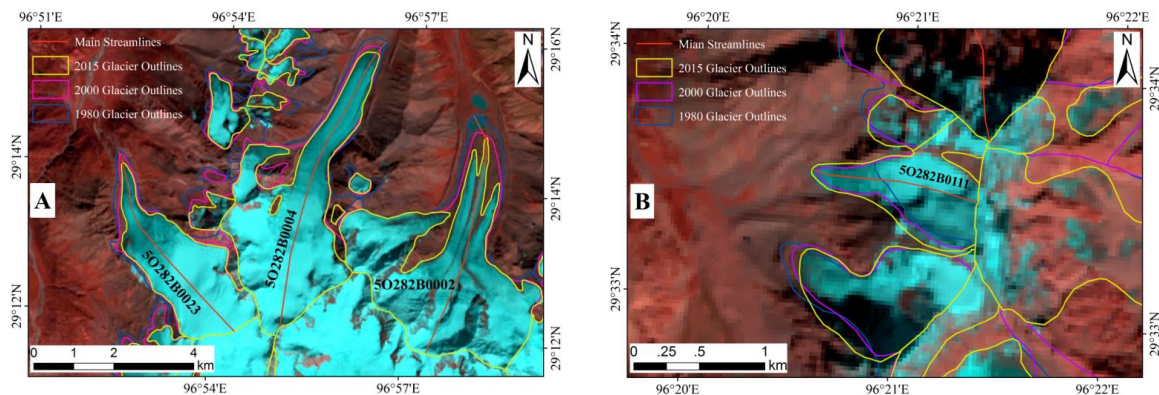
- 1 Ye, Q., Bolch, T., Naruse, R., Wang, Y., Zong, J., Wang, Z., Zhao, R., Yang, D., and Kang, S.: Glacier
2 mass changes in Rongbuk catchment on Mt. Qomolangma from 1974 to 2006 based on topographic
3 maps and ALOS PRISM data, *Journal of Hydrology*, 530, 273-280, 2015.
- 4 You, Q., Kang, S., Pepin, N., Flügel, W.-A., Yan, Y., Behrawan, H., and Huang, J.: Relationship
5 between temperature trend magnitude, elevation and mean temperature in the Tibetan Plateau from
6 homogenized surface stations and reanalysis data, *Global and Planetary Change*, 71, 124-133, 2010.
- 7 Zhang, Z., Liu, S., Wei, J., Xu, J., Guo, W., Bao, W., and Jiang, Z.: Mass Change of Glaciers in Muztag
8 Ata-Kongur Tagh, Eastern Pamir, China from 1971/76 to 2013/14 as Derived from Remote Sensing
9 Data, *PloS one*, 11, 2016a.
- 10 Zhang, Z., Xu, J.-l., Liu, S.-y., Guo, W.-q., Wei, J.-f., and Feng, T.: Glacier changes since the early
11 1960s, eastern Pamir, China, *Journal of Mountain Science*, 13, 276-291, 2016b.
- 12 Zwally, H. J., Jun, L., Brenner, A. C., Beckley, M., Cornejo, H. G., DiMARZIO, J., Giovinetto, M. B.,
13 Neumann, T. A., Robbins, J., and Saba, J. L.: Greenland ice sheet mass balance: distribution of
14 increased mass loss with climate warming; 2003–07 versus 1992–2002, *Journal of Glaciology*, 57,
15 88-102, 2011.
- 16
17
18



1
 2 Figure 1. Overview of study area and glacier distribution, including the locations of the detailed
 3 study area and meteorological stations. 96 glaciers were selected to generate centerlines and
 4 calculate length change, and then be distinguished into advanced glaciers and retreated glaciers.
 5

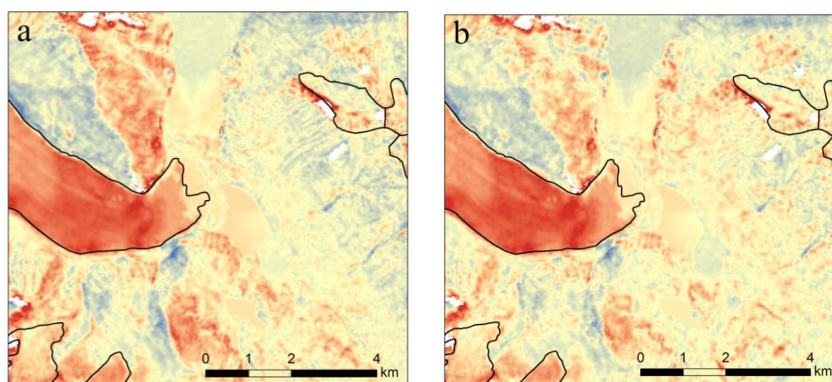


6
 7 Figure 2. Location of the detailed study area, and distribution of TOPO DEMs, TSX/TDX acquisitions
 8 and ICESat footprints. Numbers indicate specific sample glaciers.



1
 2 Figure 3. Example of glacier outlines derived from imagery collected in 1980, 2000s and 2015. The
 3 background image is Landsat OLI image (6 October 2015). (A) Examples of glacier retreat. (B) An
 4 example of glacier advance.

5
 6
 7
 8
 9
 10



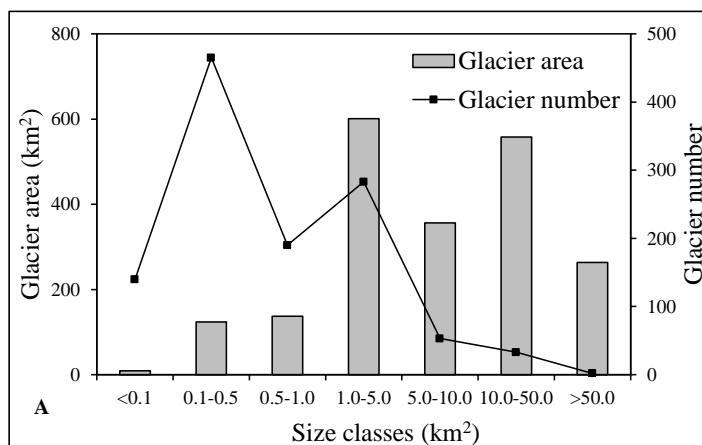
11

12 Figure 4. Elevation differences estimated between SRTM and TOPO DEM before (a) and after (b) the
 13 co-registration in the northern slope of Kangri Karpo Mountain. Location of the data example is shown
 14 in Fig. 6A.

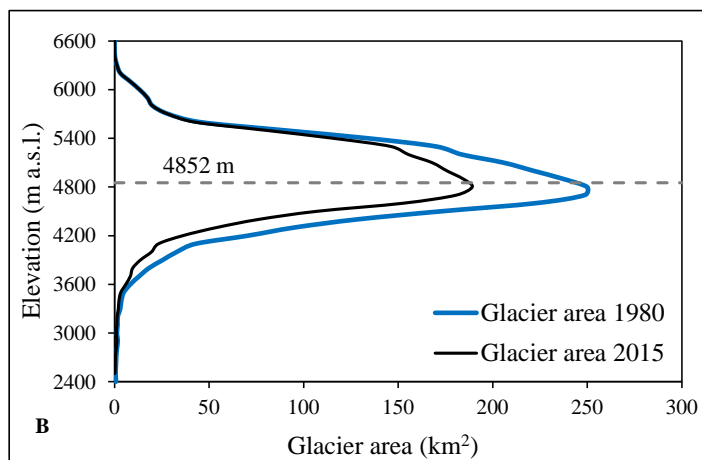
15
 16
 17
 18
 19
 20



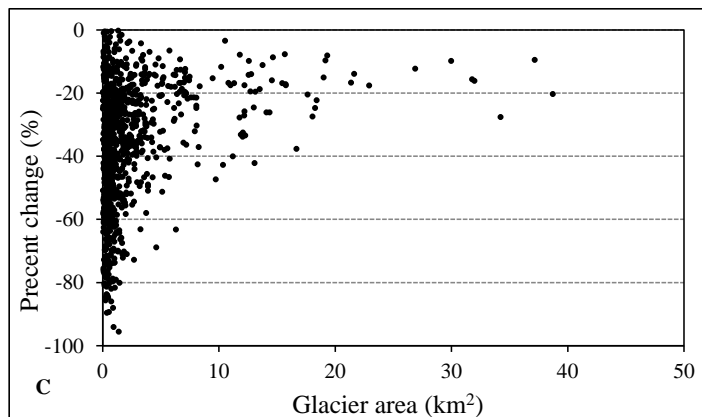
1



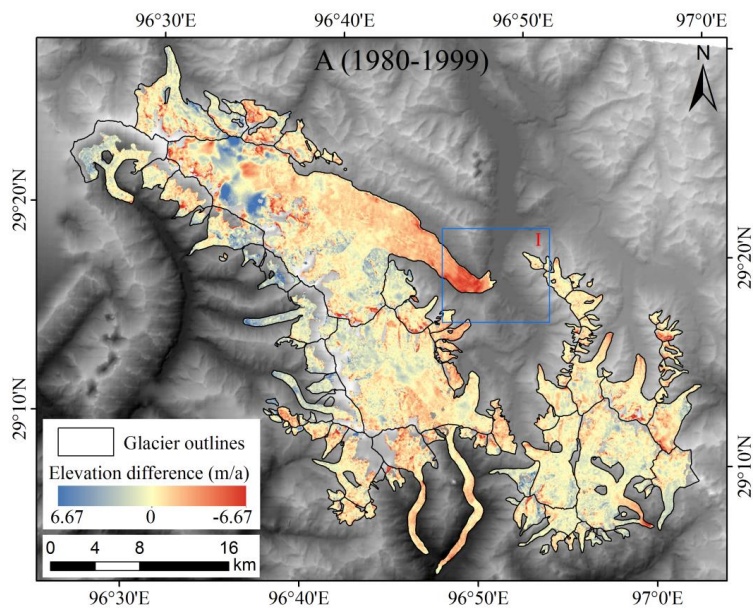
2



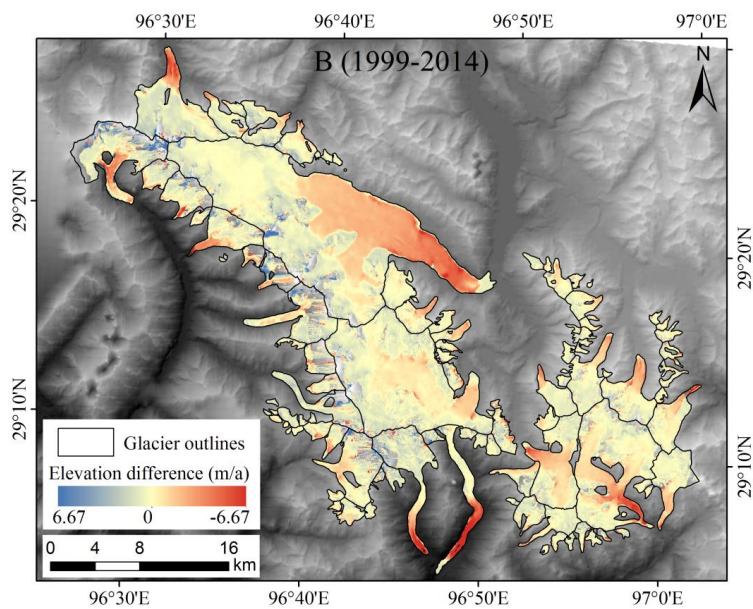
3



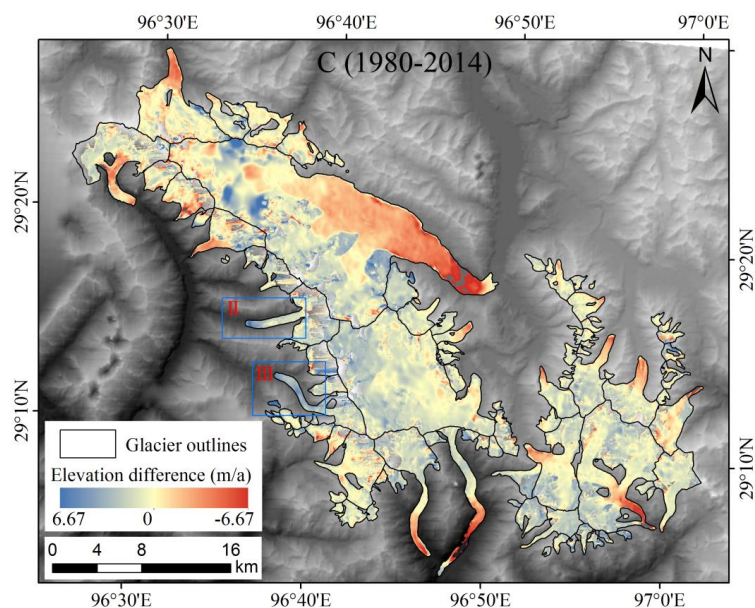
4 Figure 5. Glacier distribution and change in the Kangri Karpo Mountain. (A) Number and area of
5 glaciers in different size. (B) Percentage changes of glaciers from 1980-2015. (C) Hypsography of
6 glaciers in 1980 and 2015, the dashed line depicts value of median elevation.



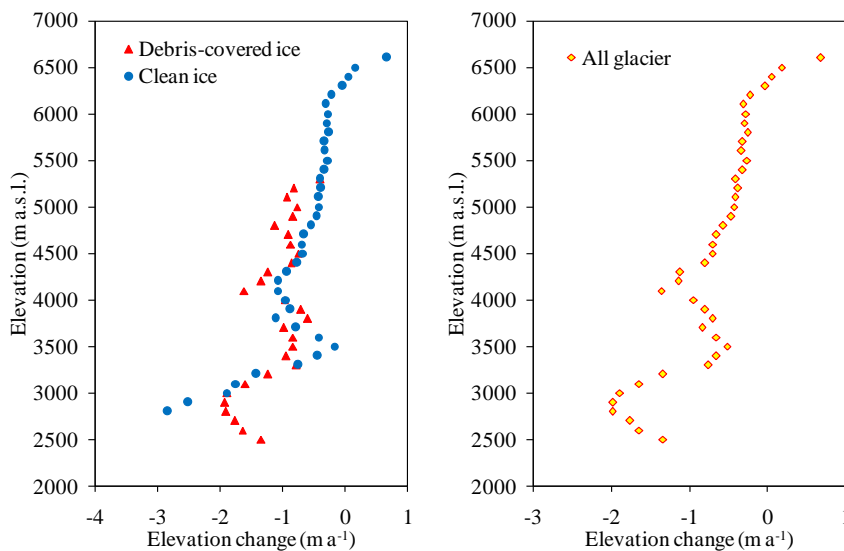
1



2



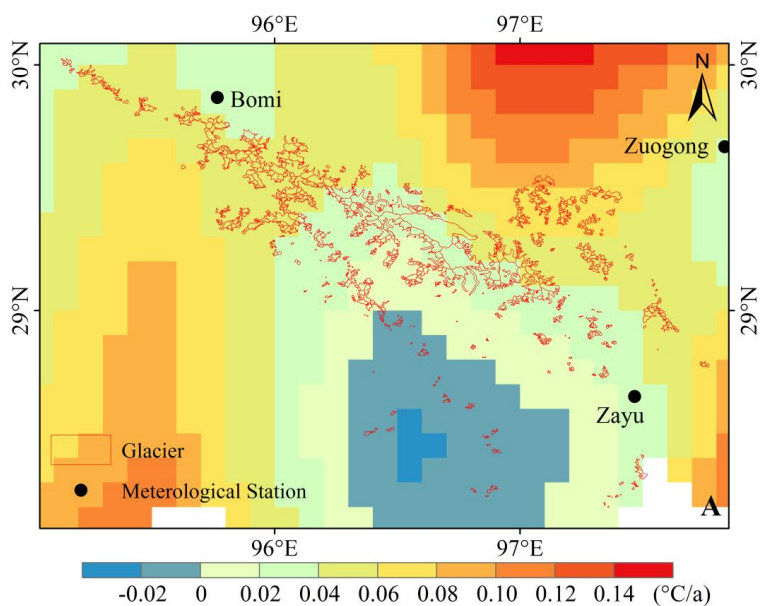
1
 2 Figure 6. Elevation changes of the detailed study area of Kangri Karpo Mountain from 1980-2014.
 3 The glacier outlines are based on the geometric union of the 1980, 2000s and 2015 glacier extent.
 4 II and III are two glaciers with positive elevation changes in glacier tongue.
 5



6
 7 Figure 7. Glacier elevation changes at each 100 m interval by altitude in the detailed study of
 8 Kangri Karpo Mountain for the clean ice, debris-covered ice and all glaciers for the period
 9 1980-2014
 10

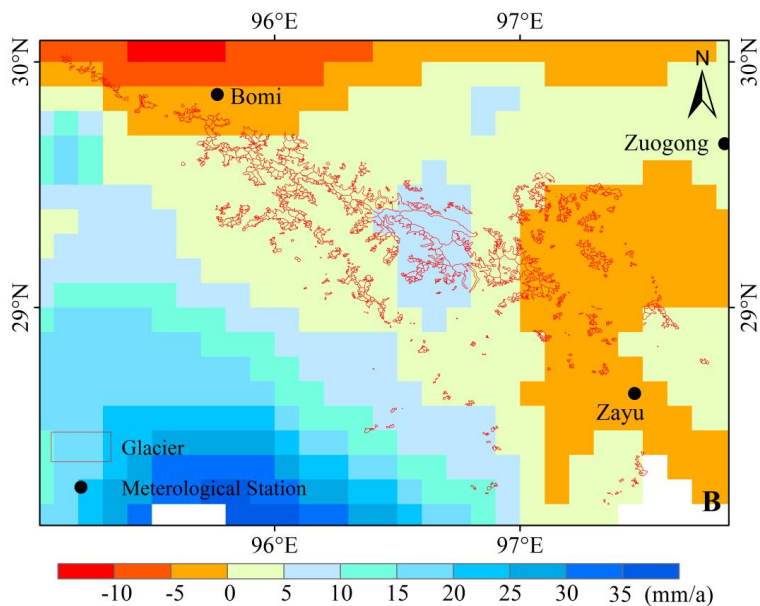


1



2

3



4

5

6

7

8

Figure 8. The changes of temperature and precipitation (from May to September) in the Kangri Karpo Mountain during 1979 - 2012. (A) temperature, (B) precipitation.



1 Table 1. Overview of satellite images and data sources.

Date	Source	ID	Pixel size (m)	Utilization
October 1980	Topographic Maps	-	12	Glacier identification for 1980
October 1980	TOPO DEM	H47e016002/H47e017002/ H47e018002 H47e016003/H47e017003/ H47e018003 H47e016004/H47e017004/ H47e018004 H47e016005/H47e017005/ H47e018005	30	Estimation of glacier elevation change
18 December 2001	Landsat TM	LT51340402001352BJC00	30	Validate and update the GAMDAM and CGI2 inventory
3 January 2002	Landsat TM	LT51340402002003BJC00	30	
23 October 2001	Landsat ETM+	LE71340402001296SGS00	15	
11-22 February 2000	SRTM C-band	-	30	Estimation of glacier elevation change
29 September 2015	Landsat OLI	LC81330402015272LGN00	15	Glacier identification for 2015
6 October 2015	Landsat OLI	LC81340402015279LGN00	15	
25 July 2015	Landsat OLI	LC81350392015206LGN00	15	
18 February 2014	TSX/TDX	TDM1_SAR_COS_BIST_SM_S_SRA _20140313T113609_20140313T113617	12	Estimation of glacier elevation change
13 March 2014	TSX/TDX	TDM1_SAR_COS_BIST_SM_S_SRA _20140313T113609_20140313T113617	12	

2

3

4 Table 2. Statistics of vertical errors between the TOPO, SRTM and TSX/TDX. MED is mean
 5 elevation difference, STDV is standard deviation, N is the number of considered pixels, SE is
 6 standard error and σ is the overall error of the derived surface elevation change.

Region	Item	MED (m)	STDV (m)	N	SE (m)	σ (m)
5O282B basin	SRTM - TOPO	-0.65	7.44	866	0.25	0.70
	TSX/TDX - SRTM	-0.90	5.83	7807	0.07	0.90
	TSX/TDX - TOPO	-1.42	5.07	7807	0.06	1.42
5O291B basin	SRTM - TOPO	0.75	8.19	963	0.26	0.80
	TSX/TDX - SRTM	0.07	12.68	8549	0.14	0.15
	TSX/TDX - TOPO	0.71	5.50	8549	0.06	0.71
Total	SRTM - TOPO	0.67	16.41	1829	0.38	0.77
	TSX/TDX - SRTM	-0.42	9.93	16356	0.08	0.43
	TSX/TDX - TOPO	-0.53	5.36	16356	0.04	0.53

7

8



Table 3. Glacier area changes in the Kangri Karpo Mountain from 1980-2015

Year	50291B basin		50291B basin		Detailed study area		Whole Mountain range	
	Area (km ²)	Change (% a ⁻¹)	Area (km ²)	Change (% a ⁻¹)	Area (km ²)	Change (% a ⁻¹)	Area (km ²)	Change (% a ⁻¹)
1980	470.31 ± 4.82		314.28 ± 4.39		784.60 ± 5.02	-	2728.00 ± 34.24	-
2000s	432.91 ± 6.31	-0.40 ± 0.08	287.97 ± 6.02	-0.42 ± 0.12	720.88 ± 7.20	-0.41 ± 0.06	-	-
2015	406.67 ± 6.76	-0.40 ± 0.14	254.46 ± 7.25	-0.78 ± 0.22	664.88 ± 7.83	-0.52 ± 0.10	2048.50 ± 48.65	-
1980-2015		-0.39 ± 0.05		-0.54 ± 0.08		-0.44 ± 0.03		-0.71 ± 0.06



Table 4. Area changes for ten sample glaciers in the detailed study area of Kangri Karpo Mountain.

ID	Glacier	WGI ID/ GLIMS ID	1980 Area			1980 - 2000			2000 - 2015			1980 - 2015		
			1980 Area (km ²)	Δa abs. (km ²)	Δa rel. (km ²)	Rate (% a ⁻¹)	Δa abs. (km ²)	Δa rel. (km ²)	Rate (% a ⁻¹)	Δa abs. (km ²)	Δa rel. (km ²)	Rate (% a ⁻¹)	Δa abs. (km ²)	Δa rel. (km ²)
1	Danong	5O282B0002/ G096960E29217N	15.46	-0.87	-5.6%	-0.28%	-1.74	-11.9%	-0.80%	-2.61	-16.9%	-0.48%		
2	Parlung NO. 4	5O282B0004/ G096920E29228N	13.52	-1.56	-11.5%	-0.58%	-0.97	-8.1%	-0.54%	-2.53	-18.7%	-0.53%		
3	Parlung NO. 10	5O282B0010/ G096904E29286N	4.98	-0.55	-11.1%	-0.55%	-0.49	-11.1%	-0.74%	-1.04	-20.9%	-0.60%		
4	Zuoqiupu	5O282B0023/ G096891E29212N	7.46	-0.76	-10.2%	-0.51%	-0.43	-6.4%	-0.43%	-1.19	-15.9%	-0.45%		
5	Bimaque	5O282B0025/ G096897E29157N	26.71	-1.25	-4.7%	-0.23%	-2.45	-9.6%	-0.64%	-3.70	-13.9%	-0.40%		
6	Xirinongpu	5O282B0028/ G096745E29216N	98.99	-2.50	-2.5%	-0.13%	-6.21	-6.4%	-0.43%	-8.71	-8.8%	-0.25%		
7	Yalong	5O282B0037/ G096657E29334N	193.43	-13.27	-6.9%	-0.34%	-7.16	-4.0%	-0.27%	-20.43	-10.6%	-0.30%		
8	/	5O291B0151/ G096711E29143N	19.17	-0.42	-2.2%	-0.11%	-1.43	-7.6%	-0.51%	-1.85	-9.6%	-0.28%		
9	/	5O291B0196/ G096943E29175N	56.45	-2.42	-4.3%	-0.21%	-6.11	-11.3%	-0.75%	-8.54	-15.1%	-0.43%		
10	/	5O291B0200/ G097005E29155N	14.66	-0.31	-2.1%	-0.10%	-0.95	-6.6%	-0.44%	-1.26	-8.6%	-0.25%		



Table 5. The length change of advanced glaciers in the Gangrigabu Range. The uncertainty of glacier length in 1980 and 2015 are 6 m and 7.5 m, and the uncertainty of length change is 0.27 m a⁻¹.

WGI ID	1980		2015		Length change (m a ⁻¹)	Lowering of terminate elevation (m)
	Length (m)	Terminate elevation (m)	Length (m)	Terminate elevation (m)		
5O282B0111	762.75	5270	1300.87	4951	15.37	319
5O282B0223	961.93	4884	1317.09	4637	10.15	247
5O282B0225	1244.88	4705	1793.16	4483	15.67	222
5O282B0226	301.13	4870	648.43	4680	9.92	190
5O282B0278	604.73	4876	707.97	4825	2.95	51
5O283A0004	1067.55	4361	2614.65	3949	44.20	412
5O283B0022	481.76	4743	625.38	4624	4.10	119
5O291A0004	342.07	4796	798.15	4762	13.03	34
5O291B0201	4045.77	3931	5047.28	3833	28.61	98
5O291B0288	1277.50	4690	1898.78	4563	17.75	127



Table 6. The length change of glaciers in the detailed study area of Kangri Karpo Mountain. The uncertainty of glacier length in 1980, 2000s and 2015 are 6 m, 7.5 m and 7.5 m, respectively. And the uncertainty of length change during 1980-2000s, 2000s-2015 and 1980-2015 are 0.48 m a^{-1} , 0.71 m a^{-1} and 0.27 m a^{-1} , respectively.

WGI ID	Glacier length (m)			Length change (m a^{-1})		
	1980	2000s	2015	1980-2000s	2000s-2015	1980-2015
5O282B0002	6271.16	5773.04	5635.20	24.91	9.19	18.17
5O282B0004	7756.96	7540.24	7375.95	10.84	10.95	10.89
5O282B0010	3167.28	2970.05	2853.12	9.86	7.80	8.98
5O282B0013	3602.30	3119.71	2960.66	24.13	10.60	18.33
5O282B0017	1631.20	1394.38	1261.97	11.84	8.83	10.55
5O282B0023	5517.39	5431.23	5209.88	4.31	14.76	8.79
5O282B0025	5357.49	4834.03	4548.90	26.17	19.01	23.10
5O282B0028	16890.03	16228.66	15817.24	33.07	27.43	30.65
5O282B0034	3925.35	3860.98	3832.31	3.22	1.91	2.66
5O282B0037	32868.46	31309.45	31105.27	77.95	13.61	50.38
5O282B0081	5306.99	5212.33	4920.24	4.73	19.47	11.05
5O282B0083	8258.42	8102.68	7921.12	7.79	12.10	9.64
5O291B0104	8209.80	8075.25	7922.90	6.73	10.16	8.20
5O291B0108	7570.99	7200.65	6725.48	18.52	31.68	24.16
5O291B0113	7677.91	7627.05	7580.98	2.54	3.07	2.77
5O291B0117	15664.48	15572.74	15456.43	4.59	7.75	5.94
5O291B0150	3509.59	2677.17	2535.09	41.62	9.47	27.84
5O291B0151	6681.68	6329.14	6309.40	17.63	1.32	10.64
5O291B0179	13104.49	13037.72	12473.61	3.34	37.61	18.02
5O291B0181	15536.55	15309.66	13137.82	11.34	144.79	68.54
5O291B0196	9241.01	7157.37	6812.94	104.18	22.96	69.37
5O291B0200	7698.33	7449.66	7013.83	12.43	29.05	19.56
5O291B0372	7681.85	7236.61	6251.62	22.26	65.67	40.86



Table 7. Mean surface elevation changes and mass balance for the single glaciers and different regions in the detailed study area of Kangri Karpo Mountain from 1980-2014. Glacier area is the geometric union of the 1980 glacier area, 2000s glacier area and 2015 glacier area. Mean ΔH is mean surface elevation changes and Mass balance is annual mass budgets.

Region	Glacier area (km ²)	1980-2000		2000-2014		1980-2014	
		Mean ΔH (m)	Mass balance (m w.e. a ⁻¹)	Mean ΔH (m)	Mass balance (m w.e. a ⁻¹)	Mean ΔH (m)	Mass balance (m w.e. a ⁻¹)
1	50282B0002	-11.05±0.70	-0.44±0.14	-13.33±0.91	-0.86±0.22	-20.66±1.42	-0.55±0.22
2	50282B0004	-7.70±0.70	-0.29±0.14	-10.16±0.91	-0.65±0.22	-15.17±1.42	-0.40±0.22
3	50282B0010	-10.31±0.70	-0.41±0.14	-10.47±0.91	-0.67±0.22	-21.44±1.42	-0.57±0.22
4	50282B0023	-6.28±0.70	-0.23±0.14	-8.71±0.91	-0.56±0.22	-14.14±1.42	-0.37±0.22
5	50282B0025	-4.24±0.70	-0.13±0.14	-13.72±0.91	-0.88±0.22	-14.52±1.42	-0.38±0.22
6	50282B0028	-5.93±0.70	-0.21±0.14	-8.90±0.91	-0.57±0.22	-10.99±1.42	-0.29±0.22
7	50282B0037	-9.21±0.70	-0.36±0.14	-15.21±0.91	-0.98±0.22	-24.51±1.42	-0.65±0.22
50282B basin	471.05	-7.92±0.70	-0.30±0.14	11.85±0.91	-0.76±0.22	-19.13±1.42	-0.51±0.22
8	50291B0151	-8.47±0.80	-0.33±0.16	-7.66±0.16	-0.49±0.04	-18.56±0.72	-0.49±0.11
9	50291B0196	-3.63±0.80	-0.11±0.16	-14.33±0.16	-0.92±0.04	-15.25±0.72	-0.40±0.11
10	50291B0200	-2.93±0.80	-0.08±0.16	-10.49±0.16	-0.67±0.04	-14.16±0.72	-0.37±0.11
50291B basin	317.22	-4.14±0.80	-0.13±0.16	-9.74±0.16	-0.63±0.04	-14.77±0.72	-0.39±0.11
Accumulation region	530.19	-4.95±0.77	-0.22±0.16	-5.69±0.43	-0.37±0.10	-12.06±0.54	-0.32±0.08
Ablation region	258.08	-5.98±0.77	-0.27±0.16	-21.00±0.43	-1.35±0.10	-27.64±0.54	-0.73±0.08
Debris-covered region	56.87	-8.87±0.77	-0.40±0.16	-27.39±0.43	-1.76±0.10	-33.50±0.54	-0.89±0.08
Clean-ice region	731.43	-5.00±0.77	-0.23±0.16	-9.70±0.43	-0.62±0.10	-16.22±0.54	-0.43±0.08
Total	788.31	-5.30±0.77	-0.24±0.16	-11.04±0.43	-0.71±0.10	-17.46±0.54	-0.46±0.08